

1 ***Suzaku* X-ray Follow-up Observations of Seven Unassociated *Fermi*-LAT Gamma-ray**
 2 **Sources at High Galactic Latitudes**

3 Y. Takahashi¹, J. Kataoka¹, T. Nakamori¹, K. Maeda¹, R. Makiya³, T. Totani³, C. C. Cheung⁴, Ł.
 4 Stawarz^{2, 5}, L. Guillemot⁶, P. C. C. Freire⁶, and I. Cognard⁷

5 s072803523@akane.waseda.jp

6 **ABSTRACT**

7 We report on our second-year campaign of X-ray follow-up observations of unidentified *Fermi*-LAT γ -ray sources at high Galactic latitudes ($|b| > 10^\circ$) using the X-ray Imaging Spectrometer onboard the *Suzaku* X-ray Observatory. In this second year of the project, seven new targets were selected from the First *Fermi*-LAT Catalog, and studied with 20–40 ks effective *Suzaku* exposures. We detected an X-ray point source coincident with the position of the recently discovered millisecond pulsar PSR J2302+4442 within the 95% confidence error circle of 1FGL J2302.8+4443. The X-ray spectrum of the detected counterpart was well fit by a blackbody model with temperature of $kT \simeq 0.3$ keV, consistent with an origin of the observed X-ray photons from the surface of a rotating magnetized neutron star. For four other targets which were also recently identified with a normal pulsar (1FGL J0106.7+4853) and millisecond pulsars (1FGL J1312.6+0048, J1902.0–5110, and J2043.2+1709), only upper limits in the 0.5–10 keV band were obtained at the flux levels of $\simeq 10^{-14}$ erg cm⁻² s⁻¹. A weak X-ray source was found in the field of 1FGL J1739.4+8717, but its association with the variable γ -ray emitter could not be confirmed with the available *Suzaku* data alone. For the remaining *Fermi*-LAT object 1FGL J1743.8–7620 no X-ray source was detected within the LAT 95% error ellipse. We briefly discuss the general properties of the observed high Galactic-latitude *Fermi*-LAT objects by comparing their multiwavelength properties with those of known blazars and millisecond pulsars.

¹Research Institute for Science and Engineering, Waseda University, 3-4-1 Okubo, Shinjuku, Tokyo, 169-8555 Japan

²Department of High Energy Astrophysics, Institute of Space and Astronautical Science (ISAS), Japan Aerospace Exploration Agency (JAXA), 3-1-1 Yoshinodai, Sagamihara, 229-8510 Japan

³Department of Astronomy, School of Science, Kyoto University, Sakyo-ku, Kyoto 606-8502

⁴National Research Council Research Associate, resident at Naval Research Laboratory, Washington, DC 20375, USA

⁵Astronomical Observatory, Jagiellonian University, ul. Orła 171, Kraków 30-244, Poland

⁶Max-Planck-Institut für Radioastronomie, Auf dem Hügel 69, 53121 Bonn, Germany

⁷Laboratoire de Physique et Chimie de l'Environnement, LPCE UMR 6115 CNRS, 45071 Orléans Cedex 02, and Station de Radioastronomie de Nançay, Observatoire de Paris, CNRS/INSU, 18330 Nançay, France

8 *Subject headings:* Stars: pulsars: general — Stars: pulsars: individual (PSR J2302+4442) —
 9 Galaxies: active — Gamma rays: general — X-rays: general

10 1. Introduction

11 Since its successful launch in 2008 June, the Large Area Telescope (LAT) onboard the *Fermi* Gamma-
 12 ray Space Telescope (Atwood et al. 2009) has enabled many important breakthroughs in the understanding
 13 of the origin of high energy γ -ray emissions of various classes of astrophysical objects. The number of
 14 detected γ -ray sources increased dramatically, from 271 objects listed in the 3rd EGRET Catalog (3EG;
 15 Hartman et al. 1999)¹ to 1873 in the Second *Fermi*-LAT Catalog (2FGL; Abdo et al. 2011). About 800
 16 γ -ray sources included in 2FGL have been identified as blazars (Ackermann et al. 2011), i.e., jetted ac-
 17 tive galactic nuclei (AGN) characterized by strong relativistic beaming. Other associations included pulsars
 18 (e.g., Abdo et al. 2010a), high-mass X-ray binaries (e.g., Abdo et al. 2009b), radio galaxies (e.g., Abdo et al.
 19 2010g), pulsar wind nebulae (e.g., Abdo et al. 2010e), supernova remnants (e.g., Abdo et al. 2010d), globu-
 20 lar clusters (e.g., Abdo et al. 2010j), starburst galaxies (e.g., Abdo et al. 2010c), and distinct objects like the
 21 Large Magellanic Cloud (Abdo et al. 2010h). However, no obvious counterparts at longer wavelengths have
 22 been found for as much as 38% of *Fermi*-LAT objects so that several hundreds of GeV sources currently
 23 remain *unassociated* with any known astrophysical systems. Fortunately, an improved localization error for
 24 the *Fermi*-LAT (typical 95% confidence radii $r_{95} \sim 0^\circ.1 - 0^\circ.2$, and even $0^\circ.005 - 0^\circ.01$ for the bright-
 25 est sources; Abdo et al. 2011), when compared to that of EGRET (typical $r_{95} \simeq 0^\circ.4 - 0^\circ.7$), allows for
 26 much more effective follow-up studies at radio, optical, and X-ray frequencies, which can help to unravel
 27 the nature of the unidentified γ -ray emitters.

28 In this context, X-ray follow-up observations of unidentified *Fermi*-LAT objects are of particular im-
 29 portance, since some classes of astrophysical sources of γ -rays such as AGN are strong X-ray emitters
 30 as well, while the others like most of γ -ray emitting pulsars are faint X-ray sources. Note that assum-
 31 ing the keV-to-GeV emission continuum in the form of a broad-band power-law ($F_\nu \propto \nu^{-\alpha_{x\gamma}}$), which
 32 could be a relatively good zero-order approximation in the case of blazar sources but not necessarily
 33 in the case of other classes of γ -ray emitters, the monochromatic X-ray flux energy density scales as
 34 $[\nu F_\nu]_{1\text{keV}} = (1\text{keV}/0.1\text{GeV})^{1-\alpha_{x\gamma}} \times [\nu F_\nu]_{0.1\text{GeV}} \simeq 3 \times 10^{-3} \times [\nu F_\nu]_{0.1\text{GeV}}$ for a relatively flat spectral
 35 index of $\alpha_{x\gamma} \simeq 0.5$. Hence, if an X-ray counterpart of a bright *Fermi*-LAT source is characterized by, e.g.,
 36 $[\nu F_\nu]_{0.1\text{GeV}} \simeq 10^{-11}\text{erg cm}^{-2}\text{s}^{-1}$ and the X-ray-to- γ -ray power-law emission continuum with the slope
 37 $\alpha_{x\gamma} \geq 0.5$, such source can be expected to be detectable with modern X-ray instruments such as *Chandra*,
 38 *XMM-Newton*, *Swift*, and *Suzaku* within reasonable exposure times. In particular, a point source search to
 39 the level of $[\nu F_\nu]_{1\text{keV}} \sim (10^{-14} - 10^{-13})\text{erg cm}^{-2}\text{s}^{-1}$ is easily attainable with the X-ray Imaging Spec-
 40 trometer (XIS; Koyama et al. 2007) onboard *Suzaku* (Mitsuda et al. 2007) with relatively short exposures of

¹See also Casandjian & Grenier (2008) for the revised catalog of EGRET γ -ray sources.

41 few tens of ksec (e.g., Akamatsu et al. 2011). In the case of a positive detection, correlated flux changes at
 42 X-ray and γ -ray frequencies provide an identification. The lack of correlated variability, or non-detection of
 43 an X-ray counterpart, provide on the other hand only circumstantial evidence regarding the nature of a stud-
 44 ied target. Yet in many cases such evidence may be crucial, since the non-detection of an X-ray counterpart
 45 despite a long, dedicated observation of a bright *Fermi*-LAT object may disprove a potential association with
 46 given classes of astrophysical sources. That is because, as mentioned above, only a few established high-
 47 energy emitters are that bright in γ -rays but very faint in X-rays (e.g., Geminga pulsar; see the discussion in
 48 Thompson 2004; Matsumoto et al. 2007).

49 Thus motivated we started a project to investigate the nature of unidentified high Galactic-latitude
 50 *Fermi*-LAT objects through deep X-ray follow-up observations with *Suzaku* XIS. The results of the first-year
 51 campaign conducted over the span of *Suzaku* AO4 were presented in Maeda et al. (2011). The AO4 program
 52 included four steady/weakly variable *Fermi*-LAT sources from the initial *Fermi*-LAT Bright Source List
 53 (0FGL; Abdo et al. 2009a) and can be summarized as follows. The X-ray counterpart for one of the bright-
 54 est unassociated *Fermi*-LAT objects, 1FGL J1231.1–1410 (also detected by EGRET as 3EG J1234–1318
 55 and EGR J1231–1412), was found. The X-ray spectrum of the counterpart was well fit by a blackbody
 56 model with a temperature of $kT \simeq 0.16$ keV plus an additional power-law component dominating above
 57 2 keV photon energies. This power-law component was confirmed in subsequent *Swift* and XMM-*Newton*
 58 exposures. Considering a recent identification of 1FGL J1231.1–1410 with the millisecond pulsar (MSP)
 59 PSR J1231–1411 (Ransom et al. 2011), in Maeda et al. we concluded that the detected thermal X-ray pho-
 60 tons originate from the surface of a rotating magnetized neutron star, while the non-thermal X-ray compo-
 61 nent is most likely produced within the pulsar magnetosphere. In the case of 1FGL J1311.7–3429, two pos-
 62 sibly associated X-ray point sources were discovered, one of which is now excluded from the smaller error
 63 ellipse of the GeV emitter as catalogued in the 2FGL (Abdo et al. 2011). The identification of the remaining
 64 X-ray counterparts with the respective γ -ray objects remain uncertain despite a robust determination of the
 65 the spectral and variability properties of the X-ray sources. In the case of 1FGL J1333.2+5056, we found
 66 several weak X-ray sources within the *Fermi*-LAT error circle, and speculated on the AGN nature of the
 67 target. Finally, one X-ray point source was detected at the edge of the error ellipse of 1FGL J2017.3+0603.
 68 The physical connection was however viewed as unlikely, since the X-ray source did not coincide with the
 69 location of the MSP PSR J2017+0603 discovered by the Nançay radio telescope which constituted a more
 70 highly probable association with the *Fermi*-LAT object (Cognard et al. 2011). The MSP identification was
 71 later indeed confirmed by the detection of the pulsed emission in the *Fermi*-LAT data, with the same period
 72 as the radio pulsations.

73 In this paper, we report the results of our second-year campaign, conducted over the span of *Suzaku*
 74 AO5 (2010 April to 2011 March) which included observations of seven *Fermi*-LAT sources located at high
 75 Galactic latitudes ($|b| > 10^\circ$). The targets were selected from the First *Fermi*-LAT Catalog of point sources
 76 (1FGL; Abdo et al. 2010b) as objects *unidentified* at the time of writing of the *Suzaku* AO5 proposal.
 77 Since then however, four of the selected targets have been associated with MSPs: 1FGL J1902.0–5110
 78 with PSR J1902–5105 (Camilo et al. 2011), 1FGL J2043.2+1709 with PSR J2043+1711 (Guillemot et al.
 79 2011), 1FGL J2302.8+4443 with PSR J2302+4442 (Cognard et al. 2011), and 1FGL J1312.6+0048 with

80 PSR J1312+00 (Abdo et al. 2011). And moreover, 1FGL J0106.7+4853 have very recently been associ-
81 ated with a normal pulsar PSR J0106+4855 (Pletsch et al. 2011). The XMM-*Newton* and *Swift* satellites
82 detected the weak X-ray counterpart of the MSP in 1FGL J2302.8+4443 (Cognard et al. 2011). In the fol-
83 lowing, our new *Suzaku* observations and data reduction procedure are described in section 2. The analysis
84 results are given in section 3, and discussed further in section 4 in the context of multiwavelength studies of
85 unidentified *Fermi*-LAT objects.

86 2. *Suzaku* Observations and Data Analysis

87 2.1. Observations and Data Reduction

88 We observed seven unidentified *Fermi*-LAT sources with the *Suzaku* XIS. These seven targets were
89 chosen from the 1FGL catalog according to the following selection criteria: (i) no association claimed at the
90 time of the submission of the *Suzaku* proposal, (ii) sources located more than $\pm 10^\circ$ away from the Galactic
91 plane, and (iii) the detection significance in the LAT γ -ray band (> 100 MeV) exceeding 14σ in the 1FGL
92 catalog. The thus selected targets are listed in Table 1 together with the corresponding *Suzaku* observation
93 logs and the 1FGL γ -ray fluxes and photon indices.

94 The observations were conducted with three XIS detector and the Hard X-ray Detector (HXD; Kokubun et al.
95 2007; Takahashi et al. 2007). The XIS detector is composed of four CCD cameras. One of the four CCD
96 cameras (XIS1) is back-illuminated CCD and the others (XIS0, XIS2, and XIS3) are front-illuminated
97 CCDs. The operation of XIS2 ceased in 2006 November because of the contamination by a leaked charge.
98 Since none of the studied sources have been detected with the HXD, below we describe the analysis of only
99 the XIS data. The XIS was operated in pointing mode and the normal clocking mode, combined with the
100 two editing modes 3×3 and 5×5 for five targets, and only one editing mode 3×3 for 1FGL J2302.8+4443
101 and 1FGL J1312.6+0048 because of the telemetry limit.

102 We conducted all the data reduction and analysis with HEADAS software version 6.9 and the calibration
103 database (CALDB) released on 2010 July 30. First, we combined the cleaned event data of the two editing
104 modes using `xselect`. Then we removed the data corresponding to the epoch of low-Earth elevation
105 angles (less than 5°), as well periods (and 60 sec after) when the *Suzaku* satellite was passing through the
106 South Atlantic Anomaly (SAA). Moreover, we also excluded the data obtained when the *Suzaku* satellite
107 was passing through the low Cut-Off Rigidity (COR) of below 6 GV. Finally we removed hot and flickering
108 pixels using `sisclean` (Day et al. 1998).

109 2.2. Data Analysis

110 X-ray images of each target were extracted from the two operating front-illuminated CCDs (XIS0 and
111 XIS3). In the image correction procedure we applied a ‘non X-ray background’ subtraction, an exposure
112 correction, and a vignetting correction (for details see Maeda et al. 2011). We then combined the images

113 from both CCDs and smoothed the thus obtained final maps using a Gaussian function with $\sigma = 0'.28$.
 114 The resulting images are presented and discussed in the next section 3. Although all the γ -ray targets were
 115 initially selected from the 1FGL catalog, in all the corresponding figures, thick green ellipses denote the
 116 more precise 95% position errors from the 2FGL catalog (Abdo et al. 2011) as described in section 2.1.

117 For the further analysis, we selected source regions around each detected X-ray source within the 2FGL
 118 error ellipses. The radii of the source extraction regions, denoted in the figures below by thin green circles,
 119 were set as $1'$, unless otherwise stated. The corresponding background regions with radii of $3'$ were taken
 120 from the low count rate area in the same XIS chips (dashed green circles). We set the detection threshold
 121 for X-ray sources at 4σ , based on the signal-to-noise ratio defined as a ratio of the excess events above a
 122 background to its standard deviation assuming a Poisson distribution. The X-ray source positions and the
 123 corresponding errors were estimated by 2D Gaussian fits, as summarized in Table 2.

124 For the timing analysis, light curves from the front-illuminated (XIS0, XIS3) and back-illuminated
 125 (XIS1) CCDs were combined; the corresponding backgrounds were subtracted using `lcmath`. The light
 126 curves constructed in this way provide the net-count rates. To quantify possible flux variations, the χ^2 test
 127 was applied to each light curve using `lcstats`. For the X-ray spectral analysis, we generated the RMF files
 128 for the detector response and the ARF files for the effective area using `xisrmfgen` and `xissimarfgen`
 129 (Ishisaki et al. 2007). In order to improve the statistics, we added X-ray counts from the two front-illuminated
 130 CCDs, using `mathpha` with no error propagation so that the resulting data follow a Poisson distribution,
 131 and then combined the response files using the `marfrmf` and `addrmf` commands. In the case of the γ -ray
 132 targets with no detected X-ray counterparts within the 2FGL error ellipses, we calculated 90% confidence
 133 level flux upper limits at the positions of the γ -ray emitters assuming an absorbed power-law model. Un-
 134 certainties of the model spectral parameters are computed at the 90% confidence levels. The results of the
 135 spectral fitting are summarized in Table 3, and discussed below in more detail.

136 3. Results

137 In this section, we first present the results of the new *Suzaku* observations in the order of R.A. for the
 138 sources for which we detected X-ray counterparts, followed by the analysis results of the remaining tar-
 139 gets with no detected X-ray counterparts. All seven targets have also recently been observed by *Swift*, and
 140 below we briefly compare the results of the *Suzaku* and *Swift* observations. We search for radio, infrared
 141 and optical counterparts for all the detected X-ray sources using the NRAO VLA Sky Survey (NVSS) cat-
 142 alog (Condon et al. 1998), the Two Micron All Sky Survey (2MASS) point source catalog (Skrutskie et al.
 143 2006), and the USNO-B1.0 catalog (Monet et al. 2003).

144 3.1. 1FGL J1312.6+0048

145 We discovered one X-ray point source inside the 2FGL error ellipse of 1FGL J1312.6+0048, at [RA,
 146 Dec]=[198°.235(2), 0°.835(2)], designated hereafter as Suzaku J1312+0050, with a detection significance

147 of 9σ (total of 178 net source counts from three detectors). This X-ray source has recently been detected also
 148 by *Swift* X-ray Telescope (XRT; Burrows et al. 2005) at [RA, Dec] = [265.4229, 0.8348] with 90% position
 149 error radius $r_{90\%} = 6''.8$. Since the position accuracy of *Swift* XRT² ($\sim 5''$) is better than that of *Suzaku* XIS
 150 ($\sim 19''$; Uchiyama et al. 2008), we searched for optical and radio counterparts of the X-ray source using
 151 the *Swift* position. We found one possibly related optical emitter USNOB 0908-0218088 at about $5''$ away
 152 from the X-ray source ([RA, Dec] = [198.241972(7), 0.83448(5)], and magnitudes B2 = 19.80, R2 = 19.32,
 153 and I = 18.11), while no radio and infrared counterparts were discovered.

154 The light curve of *Suzaku* J1312+0050 with a time bin of 5774 s and its spectrum are presented in
 155 Figures 2 and 3, respectively. The X-ray spectrum when fitted with an absorbed power-law model returned
 156 negligible hydrogen column density. We therefore fixed $N_{\text{H}} = 0$ and repeated a power-law fit obtaining
 157 the photon index of $\Gamma = 1.9_{-0.3}^{+0.4}$ with $\chi^2/\text{d.o.f.} = 9.9/13$. The derived energy flux in the 2 – 10 keV photon
 158 energy range is $8.0_{-2.6}^{+2.9} \times 10^{-14} \text{ erg cm}^{-2} \text{ s}^{-1}$. To test for flux variability, we performed a χ^2 fit with a
 159 constant count rate of $1.02 \times 10^{-1} \text{ ct s}^{-1}$ resulting in $\chi^2/\text{d.o.f.} = 14.5/7$. This indicates that the X-ray source
 160 is variable on the timescale of a few hours, with a probability of $\simeq 96\%$.

161 The targeted γ -ray object has recently been associated with the MSP PSR J1312+00 (Abdo et al. 2011).
 162 Unfortunately, the position of the radio pulsar is still not available publicly, and hence at this moment we
 163 cannot claim nor reject the coincidence of PSR J1312+00 with the detected X-ray source. The variability
 164 revealed by the *Suzaku* data, along with the presence of an optical counterpart, implies however that the de-
 165 tected X-ray source is not likely associated with the MSP PSR J1312+00. For this reason we have evaluated
 166 the 90% confidence upper limit to the 0.5 – 2 keV and 2 – 10 keV fluxes at a random position within the
 167 2FGL error ellipse of 1FGL J1312.6+0048 (excluding *Suzaku* J1312+0050), which should correspond (at
 168 least roughly) to the upper limits for the X-ray emission of PSR J1312+00. Assuming an absorbed power-
 169 law model with $n_{\text{H}} = 2.1$ (this value is taken from the LAB Survey of Galactic HI; Kalberla et al. 2005) and
 170 photon index $\Gamma = 2$, these read as $< 1.3 \times 10^{-13} \text{ erg cm}^{-2} \text{ s}^{-1}$ (0.5–2 keV) and $< 9.3 \times 10^{-14} \text{ erg cm}^{-2} \text{ s}^{-1}$
 171 (2 – 10 keV), respectively. The implied ratio of the 0.1 – 100 GeV and 2 – 10 keV fluxes $F_{\gamma}/F_{\text{X}} > 211$
 172 would be then in agreement with the pulsar association of 1FGL J1312.6+0048 (see Marelli et al. 2011).

173 3.2. 1FGL J1739.4+8717

174 We detected one X-ray source within the 2FGL error ellipse of 1FGL J1739.4+8717 (designated as
 175 *Suzaku* J1742+8715). The detection significance is 7σ (total of 204 net source counts from three detectors).
 176 The XIS image of *Suzaku* J1742+8715 seems to be relatively diffuse. However, *Swift* XRT has detected
 177 recently the same X-ray emitter as a point source at [RA, Dec] = [265.430, 87.245] with 90% position error
 178 radius $r_{90\%} = 6''.9$. Hence we conclude that in a relatively short *Suzaku* exposure (16.7 ksec) the apparently
 179 diffuse structure of the object is just an artifact of a low photon statistics. We found several weak optical
 180 sources coinciding positionally with the X-ray source, but no radio counterpart.

²See *Swift* Technical Handbook (<http://heasarc.nasa.gov/docs/swift/proposals/appendix.f.html>)

181 We extracted the source photons from a $2'$ radius circle around Suzaku J1742+8715 and the background
 182 photons from a $3'$ radius circle. The resulting X-ray spectrum and X-ray light curve with the time bin of
 183 5760 s are shown in Figures 5 and 6, respectively. A constant fit to the light curve of the X-ray source
 184 returned $\chi^2/\text{d.o.f.} = 1.9/6$, indicating that the flux was steady during the *Suzaku* exposure with the χ^2
 185 probability of $> 93\%$. The spectrum was initially fitted by an absorbed power-law model ($\chi^2/\text{d.o.f.} =$
 186 11.4/12) and this model returned $N_{\text{H}} = 0$. We then refit the spectrum after fixing the N_{H} value to zero and
 187 obtained a photon index of $\Gamma = 2.1 \pm_{-0.4}^{+0.5}$ and the unabsorbed 2 – 10 keV flux $3.6_{-1.5}^{+2.0} \text{ erg cm}^{-2} \text{ s}^{-1}$.

188 We found one relatively bright radio source inside the 2FGL error region of 1FGL J1739.4+8717,
 189 namely NVSS J173722+871744 (~ 60 mJy at 1.4 GHz). Its position is marked with a green rhombus in Fig-
 190 ure 4. This radio source is detected at several frequencies (151 MHz and 325 MHz; see Baldwin et al. 1985;
 191 Rengelink et al. 1997, respectively), but has no obvious X-ray counterpart in our *Suzaku* data. Assuming a
 192 power-law form of the radio continuum ($F_{\nu} \propto \nu^{-\alpha_{\text{r}}}$), we calculate the spectral index of NVSS J173722+871744
 193 as $\alpha_{\text{r}} = 0.2 \pm 0.1$ from the archival data. This is, in fact, a typical radio spectral index for blazar sources
 194 (e.g., Sowards-Emmerd et al. 2005). Moreover, we also found an optical and infrared counterpart, USNOB
 195 1772-0020476 ([RA, Dec] = [264.35499(2), 87.29532(2)]), which is located only $2''.2$ away from the NVSS
 196 source with optical magnitudes, B2 = 19.30, R2 = 17.61, and I = 17.07, and 2MASS J17372480+8717433
 197 ([RA, Dec] = [264.3533(1), 87.2953(1)], and magnitudes J = 16.2, H = 15.5, and K = 15.8). This allowed
 198 us to calculate radio-to-optical and optical-to-X-ray spectral indices as $\alpha_{\text{ro}} = 0.40 \pm 0.01$ and $\alpha_{\text{ox}} > 1.77$,
 199 with the latter utilizing the X-ray flux upper limit (see Figure 16). These indices are consistent with those of
 200 so-called intermediate synchrotron peaked blazars (see Fig. 7 in Ackermann et al. 2011).

201 3.3. 1FGL J2043.2+1709

202 We found one X-ray point source within the 2FGL error ellipse of 1FGL J2043.2+1709 at the respective
 203 position [RA, Dec]=[$310^{\circ}.801(2)$, $17^{\circ}.171(2)$], designated as Suzaku J2043+1710, and a second source lo-
 204 cated on the edge of the ellipse at [RA, Dec]=[$310^{\circ}.822(3)$, $17^{\circ}.133(3)$], designated as Suzaku J2043+1707
 205 (hereafter srcA and srcB for short, respectively). These two X-ray objects are not recorded in any available
 206 X-ray source catalogs. *Swift* XRT has also detected the same two X-ray emitters. Moreover, *Swift* Ultravi-
 207 olet/Optical Telescope (UVOT; Roming et al. 2005) discovered a possible UV counterpart of srcA at [RA,
 208 Dec] = [$310.80314(6)$, $17.17286(7)$], for which we found an association with the optical source USNOB
 209 1071-0645302 ([RA, Dec] = [$310.80315(7)$, $17.17300(4)$], and magnitudes B2 = 19.89, R2 = 20.6). No ra-
 210 dio and infrared counterparts for srcA or srcB were found. The X-ray image of the targeted field is shown in
 211 Figure 7. The radio position of the MSP PSR J2043+1711 recently associated with the 1FGL J2043.2+1709
 212 is marked in the figure with a green cross centered at [RA,Dec]=[$310^{\circ}.8370129(2)$, $17^{\circ}.1913744(3)$].

213 To extract the spectra and light curves of the detected X-ray sources, we set the source regions and the
 214 background region as indicated in Figure 7. The detection significances of both sources were calculated to
 215 be 16σ (total of 397 net source counts from three detectors) and 8σ (total of 155 net source counts from three
 216 detectors), respectively. No X-ray counterpart of PSR J2043+1711 was detected in our *Suzaku* exposure.

217 The light curves of srcA and srcB with time bins of 5760 s are given in Figure 8, and the corresponding
 218 spectra are presented in Figure 9. Both light curves can be well fit by constant count rates ($\chi^2/\text{d.o.f.} = 8.5/9$
 219 and $\chi^2/\text{d.o.f.} = 2.6/9$ for srcA and srcB, respectively).

220 An absorbed power-law model provided the best fit to the spectrum of srcA, returning the photon index
 221 $\Gamma = 1.67_{-0.15}^{+0.16}$ and $\chi^2/\text{d.o.f.} = 20.4/19$. In the fit, the value of N_{H} was frozen at the Galactic value in the
 222 direction of the target taken from the LAB Survey of Galactic HI, i.e., $6.63 \times 10^{20} \text{ cm}^{-2}$ (Kalberla et al.
 223 2005). We note that the fit with the absorption column density set free returned the value for N_{H} consistent
 224 with the Galactic one. The derived unabsorbed X-ray flux of srcA in the 2 – 10 keV photon energy range
 225 is $2.1_{-0.4}^{+0.4} \times 10^{-13} \text{ erg cm}^{-2} \text{ s}^{-1}$. Similarly, the X-ray spectrum of srcB was initially fitted with an absorbed
 226 power-law model. However, this model fit returned negligible value of N_{H} and therefore we fixed $N_{\text{H}} = 0$.
 227 The best fit model with $\chi^2/\text{d.o.f.} = 8.6/10$ returned then the photon index $\Gamma = 1.6_{-0.3}^{+0.4}$ and the unabsorbed
 228 2 – 10 keV flux $9.1_{-3.0}^{+3.5} \times 10^{-14} \text{ erg cm}^{-2} \text{ s}^{-1}$.

229 Assuming a power-law model with photon index $\Gamma = 2$, we calculated upper limits (90% confidence)
 230 in the 0.5 – 2 keV and 2 – 10 keV bands at the position of PSR J2043+1711 as $< 2.4 \times 10^{-14} \text{ erg cm}^{-2} \text{ s}^{-1}$
 231 and $< 3.6 \times 10^{-14} \text{ erg cm}^{-2} \text{ s}^{-1}$, respectively. This gives the ratio of the 0.1 – 100 GeV and 2 – 10 keV
 232 fluxes $F_{\gamma}/F_{\text{X}} > 864$ which is consistent with the values claimed for the GeV-detected MSP (Marelli et al.
 233 2011).

234 3.4. 1FGL J2302.8+4443

235 One X-ray point source was discovered inside the 2FGL error ellipse of 1FGL J2302.8+4443 at the
 236 position of [RA, Dec]=[345°.695(3), 44°.707(2)] (designated as Suzaku J2302+4442). The detection signif-
 237 icance of this X-ray source was calculated as 5.35σ (total of 121 net source counts from three detectors). As
 238 shown in Figure 10, the detected X-ray source coincides with the radio position of the MSP PSR J2302+4442
 239 (green cross centered at [RA, Dec]=[345°.695748(3), 44°.706136(1)]). This MSP was recently claimed to
 240 be associated with 1FGL J2302.8+4443. No optical and infrared counterparts of the pulsar were found. In
 241 the analysis of the *Suzaku* data, the source and the background regions were set as indicated in the Figure.
 242 The light curve of the X-ray counterpart with the time bin of 11520 s is presented in Figure 11. The applied
 243 χ^2 test assuming a constant count rate gave $\chi^2/\text{d.o.f.} = 4.98/5$, indicating that the X-ray flux was steady during
 244 the *Suzaku* exposure.

245 The XIS spectrum of the detected X-ray source is shown in Figure 12. Initially, we fitted the spectrum
 246 with an absorbed power-law model. This model returned an extremely soft continuum characterized by a
 247 photon index of $\Gamma = 4.5_{-1.7}^{+2.1}$, and a rather high value of $N_{\text{H}} = 0.56_{-0.34}^{+0.68} \times 10^{22} \text{ cm}^{-2}$. This absorption
 248 value is in excess of the Galactic column density in the direction of the target, namely $0.132 \times 10^{22} \text{ cm}^{-2}$, as
 249 determined by Kalberla et al. (2005) from the LAB survey of Galactic HI. Next we applied an absorbed black
 250 body model but the model fit returned N_{H} consistent with zero. We therefore fixed $N_{\text{H}} = 0$ and obtained the
 251 best-fit ($\chi^2/\text{d.o.f.} = 3.0/11$) temperature of $kT \simeq 0.31_{-0.05}^{+0.06} \text{ keV}$ (see Figure 12). The observed X-ray flux
 252 of the source is $2.6_{-0.5}^{+0.6} \times 10^{-14} \text{ erg cm}^{-2} \text{ s}^{-1}$ in the 0.5 – 2 keV range and $3.3_{-2.0}^{+2.7} \times 10^{-15} \text{ erg cm}^{-2} \text{ s}^{-1}$

253 in the 2 – 10 keV range. The ratio between γ -ray and 2 – 10 keV fluxes for 1FGL J2302.8+4443/Suzaku
 254 J2302+4442 reads as $F_\gamma/F_X = 14531$. This ratio is relatively high but still consistent with those of *Fermi*-
 255 LAT /LAT pulsars reported in Marelli et al. (2011).

256 3.5. Other Sources

257 No X-ray sources were detected in our *Suzaku* exposures inside the 2FGL error ellipses of the re-
 258 maining γ -ray objects: 1FGL J0106.7+4853, 1FGL J1743.8–7620, and 1FGL J1902.0–5110. The cor-
 259 responding X-ray images of the targets are shown in Figures 13, 14, and 15. Out of these three sources,
 260 1FGL J1902.0–5110 has been recently associated with the MSP PSR J1902–5105. Even more recently,
 261 after the submission of this paper, also 1FGL J0106.7+4853 has been identified with a new γ -ray pulsar
 262 PSR J0106+4855 (Pletsch et al. 2011). Thus only 1FGL J1743.8–7620 remains at the moment unasso-
 263 ciated. We calculated an X-ray upper limit in the 2 – 10 keV band for the latter source assuming X-ray
 264 emission from a point source located at the center of 2FGL error region, obtaining in this way the energy
 265 flux $< 4.5 \times 10^{-14} \text{ erg cm}^{-2} \text{ s}^{-1}$. In the case of 1FGL J1902.0–5110, we set the X-ray extraction region as
 266 a 1' radius circle around the radio position of PSR J1902–5105. The resulting X-ray upper limits are calcu-
 267 lated as $< 2.0 \times 10^{-14} \text{ erg cm}^{-2} \text{ s}^{-1}$ (0.5–2 keV) and $< 2.5 \times 10^{-14} \text{ erg cm}^{-2} \text{ s}^{-1}$ (2–10 keV) by assuming
 268 an absorbed power-law model with photon index $\Gamma = 2$. Finally, X-ray upper limits for 1FGL J0106.7+4853
 269 were calculated for a circular extraction region with radius 1' around the position of PSR J0106+4855, ob-
 270 taining $< 7.7 \times 10^{-15} \text{ erg cm}^{-2} \text{ s}^{-1}$ (0.5–2 keV) and $< 1.0 \times 10^{-14} \text{ erg cm}^{-2} \text{ s}^{-1}$ (2–10 keV). For these
 271 two pulsars, the ratio of the 0.1 – 100 GeV and 2 – 10 keV fluxes are $F_\gamma/F_X > 976$ and $F_\gamma/F_X > 2640$,
 272 respectively. These flux ratios are consistent with the ratios of *Fermi*-LAT pulsars reported in Marelli et al.
 273 (2011). The results of the *Swift* observations of all of the three targeted γ -ray emitters are consistent with
 274 the *Suzaku* results.

275 4. Discussion and Conclusions

276 In this paper, we report on the results of X-ray follow-up observations of seven bright *Fermi*-LAT
 277 sources at high Galactic latitudes ($|b| > 10^\circ$) using *Suzaku* XIS. We discovered the X-ray counterpart
 278 of 1FGL J2302.8+4443 coinciding with the position of the MSP PSR J2302+4442 recently claimed to
 279 be associated with the γ -ray emitter. We did not however, detect X-ray counterparts for the other four
 280 *Fermi*-LAT objects similarly identified with a normal pulsar (1FGL J0106.7+4853) and MSPs, namely for
 281 1FGL J1312.6+0048, 1FGL J1902.0–5110 and 1FGL J2043.2+1709. (In a few cases the X-rays sources
 282 have been detected within the 2FGL error ellipses, but none at the positions of the pulsars.) A relatively
 283 weak X-ray source was found inside the 2FGL error region of 1FGL J1739.4+8717. Finally, no candidate
 284 for the X-ray counterpart was detected for the remaining object 1FGL J1743.8–7620.

285 Including our previous observations of 1FGL J1231.1–1410, 1FGL J1311.7–3429, 1FGL J1333.2+5056,
 286 and 1FGL J2017.3+0603 reported in Maeda et al. (2011), our sample of high Galactic-latitude *Fermi*-LAT

287 objects initially selected as unidentified and studied with *Suzaku* consists now of eleven targets. For eight
 288 of these, we have detected single or multiple X-ray sources within the LAT error ellipses. Over the time
 289 period when the *Suzaku* observations were being obtained, six targets from the γ -ray sample were found
 290 to be associated with MSPs, one target (1FGL J0106.7+4853) has been associated with a normal pulsar,
 291 and one source (1FGL J1333.2+5056) has been classified as an AGN candidate, all in agreement with the
 292 gathered X-ray data. Still, four objects from the list remain unidentified. As argued below, one of these four,
 293 1FGL J1739.4+8717, is quite likely a high-redshift blazar.

294 The source 1FGL J1739.4+8717 was characterized by an enhanced flux level within the LAT photon
 295 energy range during the the first seven months of *Fermi*-LAT operation³. After that time, the activity of the γ -
 296 ray emitter decreased. The photon index in the LAT energy band is $\Gamma_\gamma = 2.1 \pm 0.1$ (where $dN/dE \propto E^{-\Gamma_\gamma}$ is
 297 the differential photon flux; Abdo et al. 2011), which is a typical value for the γ -ray spectra of BL Lac type
 298 blazars (see Ackermann et al. 2011). Importantly, as written in section 3.2 one relatively bright radio source,
 299 NVSS J173722+871744, is located inside the 2FGL error region of 1FGL J1739.4+8717 (see Figure 4).
 300 With a typical radio spectral index for blazar sources and radio-to-optical and optical-to-X-ray spectral
 301 indices that are consistent with blazar broadband spectrum, it is quite likely that 1FGL J1739.4+8717 is
 302 indeed associated with a distant blazar currently characterized by an activity level low enough so that its
 303 X-ray emission was below the detection limit of the XIS instrument ($\sim 10^{-15}$ erg cm⁻² s⁻¹) at the time of
 304 the performed *Suzaku* observations.

305 In general, unidentified sources constituted a large fraction of the population of γ -ray emitters detected
 306 by EGRET ($\sim 60\%$ in 3EG), and at present about 31 % of *Fermi*-LAT sources in 2FGL catalog remain
 307 unassociated (specifically 273 sources at high Galactic latitudes ($|b| > 10^\circ$) and 303 sources at low Galactic
 308 latitudes $|b| < 10^\circ$). Those located at the lowest Galactic latitudes ($|b| < 5^\circ$) are most widely expected to be
 309 associated with local systems such as molecular clouds, supernova remnants, massive stars, high-mass X-ray
 310 binaries, radio quiet pulsars, and pulsar wind nebulae (e.g., Kaaret & Cottam 1996; Yadigaroglu & Romani
 311 1997; Romero et al. 1999). In particular, half a dozen of the brightest 3EG sources in the Galactic plane were
 312 identified as young pulsars (Thompson et al. 1999), despite the relatively poor localization of the EGRET
 313 sources and the source confusion complicated substantially the identification procedure. On the other hand,
 314 most of the unassociated 3EG sources at high Galactic latitudes ($|b| > 10^\circ$) were later identified as blazars
 315 (Sowards-Emmerd et al. 2003, 2004). Pulsars were therefore expected to be found mainly among GeV emit-
 316 ters at low Galactic latitudes, while blazars were supposed to constitute the main population of GeV emitters
 317 at high Galactic latitudes. But the γ -ray-bright pulsars were also expected to be found at intermediate Galac-
 318 tic latitudes ($5^\circ < |b| < 73^\circ$; Crawford et al. 2006). The identification of a number of *Fermi*-LAT objects
 319 located above the Galactic plane ($|b| > 10^\circ$) with such systems (predominantly with MSPs) confirmed
 320 these expectations (see, e.g., Ransom & Pulsar Search Consortium 2010, and the discussion in Maeda et al.
 321 2011).

322 In Figure 17 we plot the X-ray-to- γ -ray energy flux density ratios ($F_{2-10\text{ keV}}/F_{0.1-100\text{ GeV}}$) versus
 323 radio-to- γ -ray energy flux density ratios ($F_{1.4\text{ GHz}}/F_{0.1-100\text{ GeV}}$) for the *Fermi*-LAT objects from our *Suzaku*

³<http://heasarc.gsfc.nasa.gov/FTP/fermi/data/lat/catalogs/source/lightcurves/2FGLJ1738.9+8716.png>

324 sample discussed here (blue circles) with the radio data available in the literature (Abdo et al. 2010b;
 325 Condon et al. 1998, see Table 3). These can be compared with the analogous ratios evaluated for bright
 326 *Fermi*-LAT objects identified with blazars and MSPs (denoted in the figure by red crosses and squares, re-
 327 spectively). We remind the reader that the blazar class includes flat spectrum radio quasars (FSRQs) and
 328 BL Lacertae objects (BL Lacs). In addition, in the figure we plot the two targets discussed in Maeda et al.
 329 (2011), namely 1FGL J1333.2+5056 most likely associated with an AGN, and a peculiar object 1FGL J1311.7–3429
 330 (pink stars). As shown, the blazar and MSP populations are clearly separated in the constructed flux ra-
 331 tio plane. Also, four objects from our sample which have recently been associated with a normal pulsar
 332 (1FGL J0106.7+4853) and MSPs (1FGL J1312.6+0048, 1FGL J2043.2+1709, and 1FGL J2302.8+4443)
 333 occupy the same region in the analyzed parameter space as the previously known MSPs detected in the GeV
 334 range⁴. On the other hand, in the case of 1FGL J1739.4+8717 the evaluated energy flux density ratios —
 335 which are very similar to those characterizing 1FGL J1333.2+5056 — are consistent with the blazar iden-
 336 tification proposed above, if only NVSS J173722+871744 is considered as the true counterpart of the γ -ray
 337 emitter.

338 In all, we conclude that the gathered *Suzaku* XIS data together with the broad-band properties of
 339 the analyzed *Fermi*-LAT objects are in agreement with the identification of most of them as MSPs. Yet
 340 a few cases in the analyzed sample (1FGL J1739.4+8717, 1FGL J1333.2+5056) constitute quite proba-
 341 ble associations with AGN (high-redshift blazars). Finally, the nature of the remaining few targets (like
 342 1FGL J1311.7–3429) is still an open question, although, as inferred from Figure 17, the MSP identifica-
 343 tion seems more viable than the blazar one. In the near future, we are further continuing our X-ray studies
 344 during the *Suzaku* AO6 cycle, focusing on both new targets (1FGL J0103.1+4840, 1FGL J1946.7–5404,
 345 and 1FGL J2339.7–0531), but also performing ultra-deep exposures on particularly intriguing sources like
 346 1FGL J1311.7-3429.

347 Finally, let us comment in more detail on the case of 1FGL J2302.8+4443. This object, as already
 348 mentioned above, has recently been associated with the millisecond pulsar PSR J2302+4442 discovered by
 349 the Nançay radio telescope (Cognard et al. 2011). The rotation period of the pulsar is $P \simeq 5.19$ ms, the spin-
 350 down luminosity is $\dot{E} \simeq 3.74 \times 10^{33}$ erg s⁻¹, and the characteristic age can be evaluated as $\tau \simeq 6.2$ Gyr.
 351 Cognard et al. (2011) reported also on the detection of the X-ray counterpart of the pulsar with XMM-
 352 *Newton*, with the unabsorbed 0.5 – 3 keV flux of $3.1_{-0.4}^{+0.4} \times 10^{-14}$ erg cm⁻² s⁻¹. This is consistent with our
 353 *Suzaku* detection (the re-calculated flux in the same photon energy range $2.9_{-1.2}^{+1.1} \times 10^{-14}$ erg cm⁻² s⁻¹).
 354 Anticipating the distance of the pulsar $d \simeq 1.18$ kpc which was inferred from the NE2001 model of Galactic
 355 free electron density (Cordes & Lazio 2001), the X-ray luminosity of PSR J2302+4442 can therefore be
 356 evaluated roughly as $L_x \sim 3 \times 10^{30}$ erg s⁻¹. This, together with \dot{E} provided above, is then in good agreement
 357 with the scaling relation between the X-ray and spin-down luminosities $L_x \sim 10^{-3} \times \dot{E}$ established for
 358 MSPs (Becker & Truemper 1997; Gaensler & Slane 2006; Zhang et al. 2007), although the inferred distance

⁴In the case of 1FGL J1312.6+0048, the X-ray-to- γ -ray energy flux density ratio shown in Figure 17 is evaluated assuming the association of the γ -ray sources with the MSP PSR J1312+00. That is, the *Suzaku* XIS upper limit derived at the position of the pulsar is considered, and not the X-ray flux of the *Suzaku* source detected within 2FGL error region.

359 of PSR J2302+4442 is indicated to be smaller by a factor of four considering an unphysically high γ -ray
360 efficiency and, instead, assuming average efficiency of γ -ray MSPs $\sim 10\%$ (Cognard et al. 2011).

361 The spectrum of the X-ray counterpart of PSR J2302+4442/1FGL J2302.8+4443 was well fit by a
362 blackbody model, and this is again in agreement with the idea that the observed X-ray photons originate
363 from thermal emission from the surface of a rotating magnetized neutron star. Because of the limited photon
364 statistics in the higher energy range of XIS, we could not however confirm the presence of a non-thermal
365 component above 2 keV (clearly detected in the case of 1FGL J1231.1–1410 by Maeda et al. 2011). Inter-
366 estingly, for the isolated pulsars as old as PSR J2302+4442 (characteristic age of about 6 Gyr), the surface
367 temperature of the neutron star is expected to be $T \lesssim 10^5$ K (Nomoto & Tsuruta 1987; Page & Applegate
368 1992). Our detection of the X-ray counterpart indicated $kT \simeq 0.31 \pm 0.03$ keV, i.e. $T \simeq 3.6 \times 10^6$ K instead.
369 Some reheating process is therefore required, possibly related to the impact of relativistic particles on polar
370 caps (Becker & Truemper 1997, and references therein).

371 C.C. Cheung’s work at NRL is sponsored by NASA DPR S-15633-Y. Ł.S. is grateful for the support
372 from Polish MNiSW through the grant N-N203-380336. We thank the anonymous referee for a careful
373 reading of the manuscript and useful suggestion which helped to improve the paper.

374 REFERENCES

- 375 Abdo, A. A., Ackermann, M., Ajello, M., et al. 2009a, ApJS, 183, 46
376 Abdo, A. A., Ackermann, M., Ajello, M., et al. 2009b, ApJ, 701, L123
377 Abdo, A. A., Ackermann, M., Ajello, M., et al. 2010a, ApJS, 187, 460
378 Abdo, A. A., Ackermann, M., Ajello, M., et al. 2010b, ApJS, 188, 405
379 Abdo, A. A., Ackermann, M., Ajello, M., et al. 2010c, ApJ, 709, L152
380 Abdo, A. A., Ackermann, M., Ajello, M., et al. 2010d, ApJ, 710, L92
381 Abdo, A. A., Ackermann, M., Ajello, M., et al. 2010e, ApJ, 714, 927
382 Abdo, A. A., Ackermann, M., Agudo, I., et al. 2010f, ApJ, 716, 30
383 Abdo, A. A., Ackermann, M., Ajello, M., et al. 2010g, ApJ, 720, 912
384 Abdo, A. A., Ackermann, M., Ajello, M., et al. 2010h, A&A, 512, A7
385 Abdo, A. A., Ackermann, M., Ajello, M., et al. 2010i, A&A, 524, A75
386 Abdo, A. A., Ackermann, M., Ajello, M., et al. 2010j, Sci, 325, 848
387 Abdo, A. A., Ackermann, M., Ajello, M., et al. 2011, submitted, arXiv:1108.1435

- 388 Ackermann, M., Ajello, M., Allafort, A., et al. 2011, submitted, arXiv:1108.1420
- 389 Akamatsu, H., Hoshino, A., Ishisaki, Y., et al. 2011, arXiv:1106.5653
- 390 Atwood, W. B., Abdo, A. A., Ackermann, M., et al. 2009, *ApJ*, 697, 1071
- 391 Bailes, M., Johnston, S., Bell, J. F., et al. 1997, *ApJ*, 481, 386
- 392 Baldwin, J. E., Boysen, R. C., Hales, S. E. G., et al. 1985, *MNRAS*, 217, 717
- 393 Becker, W., & Truemper, J. 1997, *A&A*, 326, 682
- 394 Burrows D. N., Hill, J. E., Nousek, J. A., et al. 2005, *Space Science Reviews*, 120 165
- 395 Casandjian, J.-M., & Grenier, I. A. 2008, *A&A*, 489, 849
- 396 Camilo, F., et al. 2011, in prep.
- 397 Cognard, I., et al. 2011, in prep.
- 398 Condon, J. J., Cotton, W. D., Greisen, E. W., et al. 1998, *AJ*, 115, 1693
- 399 Cordes, J. M., & Lazio, T. J. W. 2001, *ApJ*, 549, 997
- 400 Crawford, F., Roberts, M. S. E., Hessels, J. W. T., et al. 2006, *ApJ*, 652, 1499
- 401 Day, C., et al. 1998, *The ASCA Data Reduction Guide*, Tech. Rep., (Greenbelt: NASA GSFC), v.2.0
- 402 Gaensler, B. M., & Slane, P. O. 2006, *ARA&A*, 44, 17
- 403 Guillemot, L., Freire, P. C. C., Cognard, I., et al. 2012, *MNRAS*, submitted
- 404 Hartman, R. C., Bertsch, D. L., Bloom, S. D., et al. 1999, *ApJS*, 123, 79
- 405 Ishisaki, Y., Maeda, Y., Fujimoto, R., et al. 2007, *PASJ*, 59, 113
- 406 Kaaret, P., & Cottam, J. 1996, *ApJ*, 462, L35
- 407 Kalberla, P. M. W., Burton, W. B., Hartmann, D., et al. 2005, *A&A*, 440, 775
- 408 Kokubun, M., Makishima, K., Takahashi, T., et al. 2007, *PASJ*, 59, 53
- 409 Koyama, K., Tsunemi, H., Dotani, T., et al. 2007, *PASJ*, 59, 23
- 410 Lundgren, S. C., Zepka, A. F., Cordes, J. M., 1995, *ApJ*, 453, 419
- 411 Maeda, K., Kataoka, J., Nakamori, T., et al. 2011, *ApJ*, 729, 103
- 412 Marelli, M., De Luca, A., & Caraveo, P. A. 2011, *ApJ*, 733, 82
- 413 Matsumoto, H., Ueno, M., Bamba, A., et al. 2007, *PASJ*, 59, 199

- 414 Mitsuda, K., Bautz, M., Inoue, H., et al. 2007, PASJ, 59, 1
- 415 Monet D. G., Levine, S. E., Canzian, B., et al. 2003, AJ, 125, 984
- 416 Navarro, J., Bruyn, A. G., Frail, D. A., et al. 1995, ApJ, 455, L55
- 417 Nomoto, K., & Tsuruta, S. 1987, ApJ, 312, 711
- 418 Page, D., & Applegate, J. H. 1992, ApJ, 394, L17
- 419 Pletsch, H. J., Guillemot, L., Allen, B., et al. 2011, arXiv:1111.0523
- 420 Ransom, S. M., & Pulsar Search Consortium, F. 2010, Bulletin of the American Astronomical Society, 42,
421 655
- 422 Ransom, S. M., Ray, P. S., Camilo, F., et al. 2011, ApJ, 727, L16
- 423 Rengelink, R. B., Tang, Y., de Bruyn, A. G., et al. 1997, A&AS, 124, 259
- 424 Romero, G. E., Benaglia, P., & Torres, D. F. 1999, A&A, 348, 868
- 425 Roming, P. W. A., Kennedy, T. E., Mason, K. O., et al. 2005, SSRv, 120, 95
- 426 Sakurai, I., Kawai, N., Torii, K., et al. 2001, PASJ, 53, 535
- 427 Skrutskie, M. F., Cutri, R. M., Stiening, R., et al. 2006, AJ, 131, 1163
- 428 Sowards-Emmerd, D., Romani, R. W., & Michelson, P. F. 2003, ApJ, 590, 109
- 429 Sowards-Emmerd, D., Romani, R. W., Michelson, P. F., & Ulvestad, J. S. 2004, ApJ, 609, 564
- 430 Sowards-Emmerd, D., Romani, R. W., Michelson, P. F., Healey, S. E., & Nolan, P. L. 2005, ApJ, 626, 95
- 431 Takahashi, T., Abe, K., Endo, M., et al. 2007, PASJ, 59, 35
- 432 Thompson, D. J. 2004, Cosmic Gamma-Ray Sources, 304, 149
- 433 Thompson, D. J., Bailes, M., Bertsch, D. L., et al. 1999, ApJ, 516, 297
- 434 Uchiyama, Y., Maeda, Y., Ebara, M., et al. 2008, PASJ, 60, 35
- 435 Webb, N. A., Olive, J.-F., Barret, D., 2004a, A&A, 417, 181
- 436 Webb, N. A., Olive, J.-F., Barret, D., et al. 2004b, A&A, 419, 269
- 437 Yadigaroglu, I.-A., & Romani, R. W. 1997, ApJ, 476, 347
- 438 Zhang, L., Fang, J., & Chen, S. B. 2007, ApJ, 666, 1165

Table 1: *Suzaku* Observation Logs and γ -ray properties of the targets

Name	OBS ID	Pointing Direction ^a		Observation start (UT)	Effective exposure [ksec]	γ -ray photon index ^b	γ -ray flux ^b $F_{0.1-100\text{GeV}}$ [erg cm ⁻² s ⁻¹]
		RA [deg]	DEC [deg]				
1FGL J0106.7+4853	705010010	16.6433	48.9425	2010/07/15 09:53:44	19.7	2.05	2.64×10^{-11}
1FGL J1312.6+0048	705011010	198.1860	0.8370	2011/01/17 04:38:43	17.5	1.99	1.96×10^{-11}
1FGL J1739.4+8717	705012010	264.8730	87.2900	2010/04/26 23:41:56	16.7	2.12	2.92×10^{-11}
1FGL J1743.8–7620	705013010	265.9610	–76.3420	2010/04/14 00:16:05	34.0	2.14	2.83×10^{-11}
1FGL J1902.0–5110	705014010	285.5220	–51.1700	2010/04/13 06:37:43	38.5	2.10	2.46×10^{-11}
1FGL J2043.2+1709	705015010	310.8220	17.1640	2010/05/03 19:23:03	17.7	2.13	3.15×10^{-11}
1FGL J2302.8+4443	705016010	345.7070	44.7230	2010/06/26 05:52:36	35.6	2.04	4.81×10^{-11}

^a The pointing directions are the values of planned target coordinates.

^b These values are taken from 1FGL catalog (Abdo et al. 2010b).

Table 2: Results of the *Suzaku* observations of the selected *Fermi*-LAT sources. Positions of detected X-ray sources are presented.

Name	Position		
	Suzaku detection	RA[deg]	DEC[deg]
1FGL J0106.7+4853	-	-	-
1FGL J1312.6+0048	SUZAKU J1312+0050	198.235(2)	0.835(2)
1FGL J1739.4+8717	source ^a	-	-
1FGL J1743.8–7620	-	-	-
1FGL J1902.0–5110	-	-	-
1FGL J2043.2+1709	SUZAKU J2043+1710	310.801(2)	17.171(2)
	SUZAKU J2043+1707	310.822(3)	17.133(3)
1FGL J2302.8+4443	PSR J2302+4442	345.695(3)	44.707(2)

^aWe could not determine the exact position of the source because of extended source image (see section 3.2).

Table 3: Results of the analysis of the *Suzaku* /XIS data and radio fluxes of the sources

Name		N_{H} [10^{20} cm^{-2}]	Model	Model parameter	X-ray flux $F_{2-10\text{keV}}$ [$\text{erg cm}^{-2} \text{ s}^{-1}$]	Radio flux $F_{1.4\text{GHz}}$ [mJy]
1FGL J0106.7+4853	PSR J0106+4855	11.9 (fixed)	PL	$\Gamma=2.0$ (fixed)	$< 1.0 \times 10^{-14}$	< 0.008
1FGL J1312.6+0048	source	0.0 (fixed)	PL	$\Gamma=1.9^{+0.4}_{-0.3}$	$8.0^{+2.9}_{-2.6} \times 10^{-14}$	< 0.71
	off-source ^c	2.1 (fixed)	PL	$\Gamma=2.0$ (fixed)	$< 9.3 \times 10^{-14}$	< 0.82
1FGL J1739.4+8717	source	6.36 (fixed)	PL	$\Gamma=2.1^{+0.5}_{-0.4}$	$3.6^{+2.0}_{-1.5} \times 10^{-13}$	< 0.58
	NVSS J173722+871744	6.4 (fixed)	PL	$\Gamma=2.0$ (fixed)	$< 1.5 \times 10^{-14}$	61.3
1FGL J1743.8–7620	-	8.13 (fixed)	PL	$\Gamma=2.0$ (fixed)	$< 4.5 \times 10^{-14}$	-
1FGL J1902.0–5110	PSR J1902-5105	4.87 (fixed)	PL	$\Gamma=2.0$ (fixed)	$< 2.5 \times 10^{-14}$	-
1FGL J2043.2+1709	src A	6.63 (fixed)	PL	$\Gamma=1.67^{+0.16}_{-0.15}$	$2.1^{+0.4}_{-0.4} \times 10^{-13}$	< 1.01
	src B	0.0 (fixed)	PL	$\Gamma=1.6^{+0.4}_{-0.3}$	$9.1^{+3.5}_{-3.0} \times 10^{-14}$	< 1.00
	PSR J2043+1711	6.67 (fixed)	PL	$\Gamma=2.0$ (fixed)	$< 3.6 \times 10^{-14}$	0.01^a
1FGL J2302.8+4443	PSR J2302+4442	0.0 (fixed)	BB	$kT=0.31^{+0.06}_{-0.05} \text{ keV}$	$3.3^{+2.7}_{-2.0} \times 10^{-15}$	1.2^b

Note. —Summary of analysis results of the seven studied 1FGL sources. Unabsorbed X-ray flux and 90 % confidence upper limits in the 2–10 keV band for all the sources are listed. The X-ray upper limits are calculated assuming a power law model with a photon index of 2 for the 1FGL sources with no X-ray detection. In the seventh column, radio fluxes or upper limits at 1.4 GHz are presented. Radio fluxes and upper limits The radio values with no footnote marks were taken either directly from the NVSS (Condon et al. 1998) catalog (for NVSS J173722+871744) or measured by us from the NVSS images (the upper limits; 90% confidence levels).

^a This value is estimated by averaging the radio flux over four observations during which the pulsar was detected.

^b From Cognard et al. (2011).

^c The evaluated off-source X-ray upper limits expected to represent MSP PSR J1312+00.

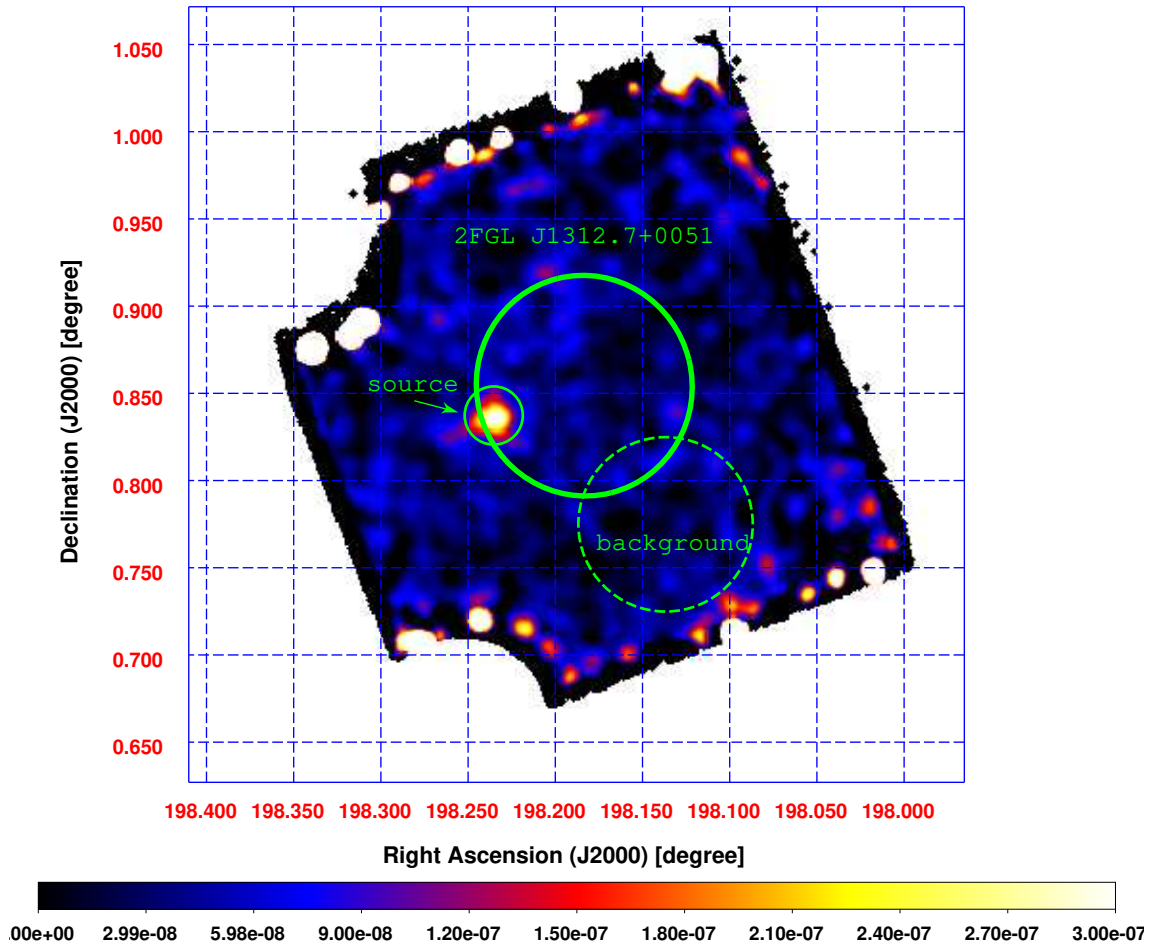


Fig. 1.— X-ray image of 1FGL J1312.6+0048 by *Suzaku*/XIS0+3 (FI CCDs) in the 0.5 to 10 keV energy band. Thick solid ellipse denotes the 95% position error of 1FGL J1312.6+0048 in the 2FGL catalog. Thin solid and dashed circles show the source and background regions, respectively. The accurate position of PSR J1312+00 is still not available in the literature.

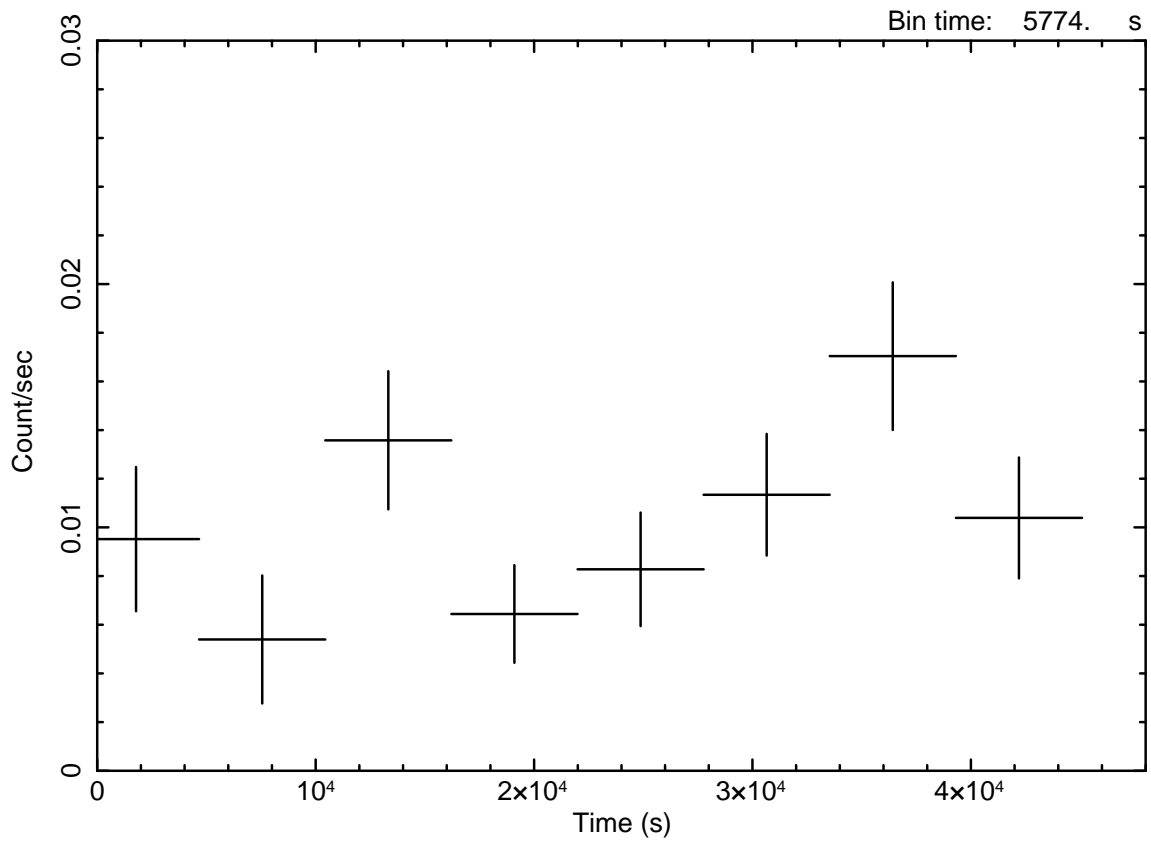


Fig. 2.— *Suzaku*/XIS light curve of the possible X-ray counterpart of 1FGL J1312.6+0048.

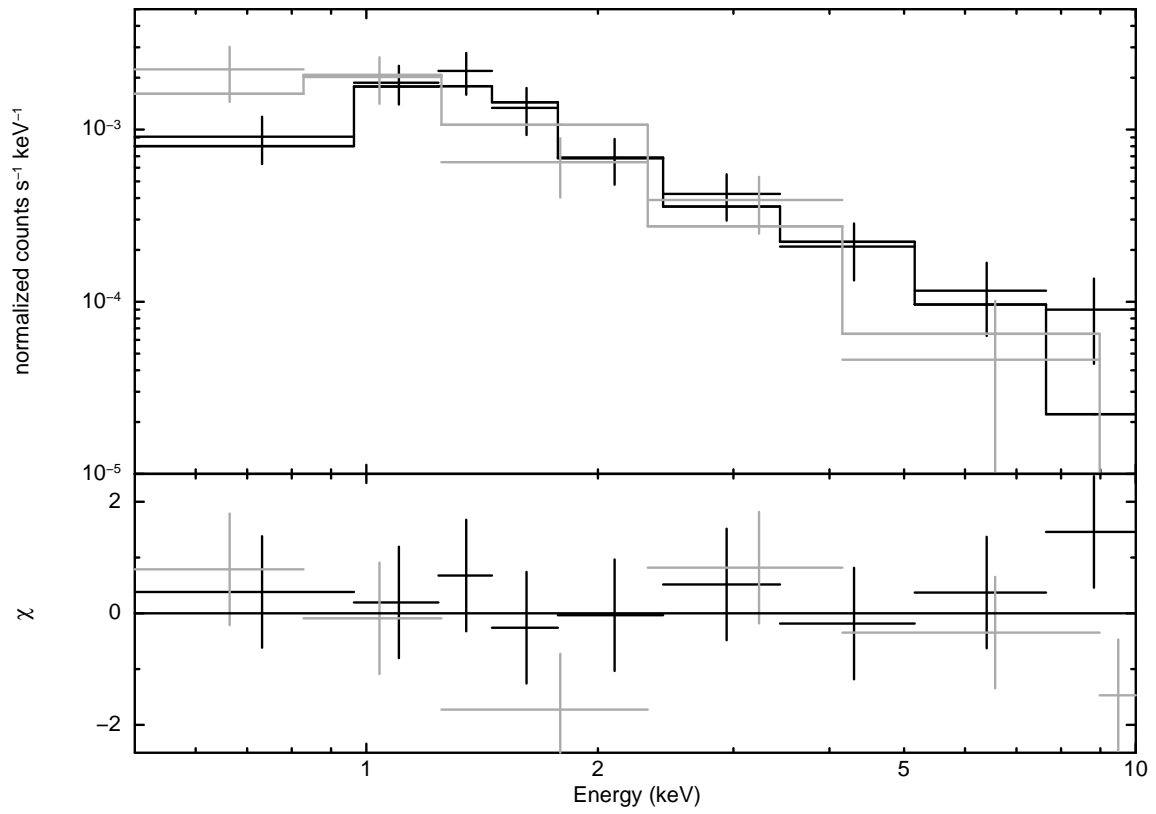


Fig. 3.— *Suzaku*/XIS spectrum of the possible X-ray counterpart for 1FGL J1312.6+0048 fitted with a power-law model. Black plots show the FI data and gray plots show the BI data.

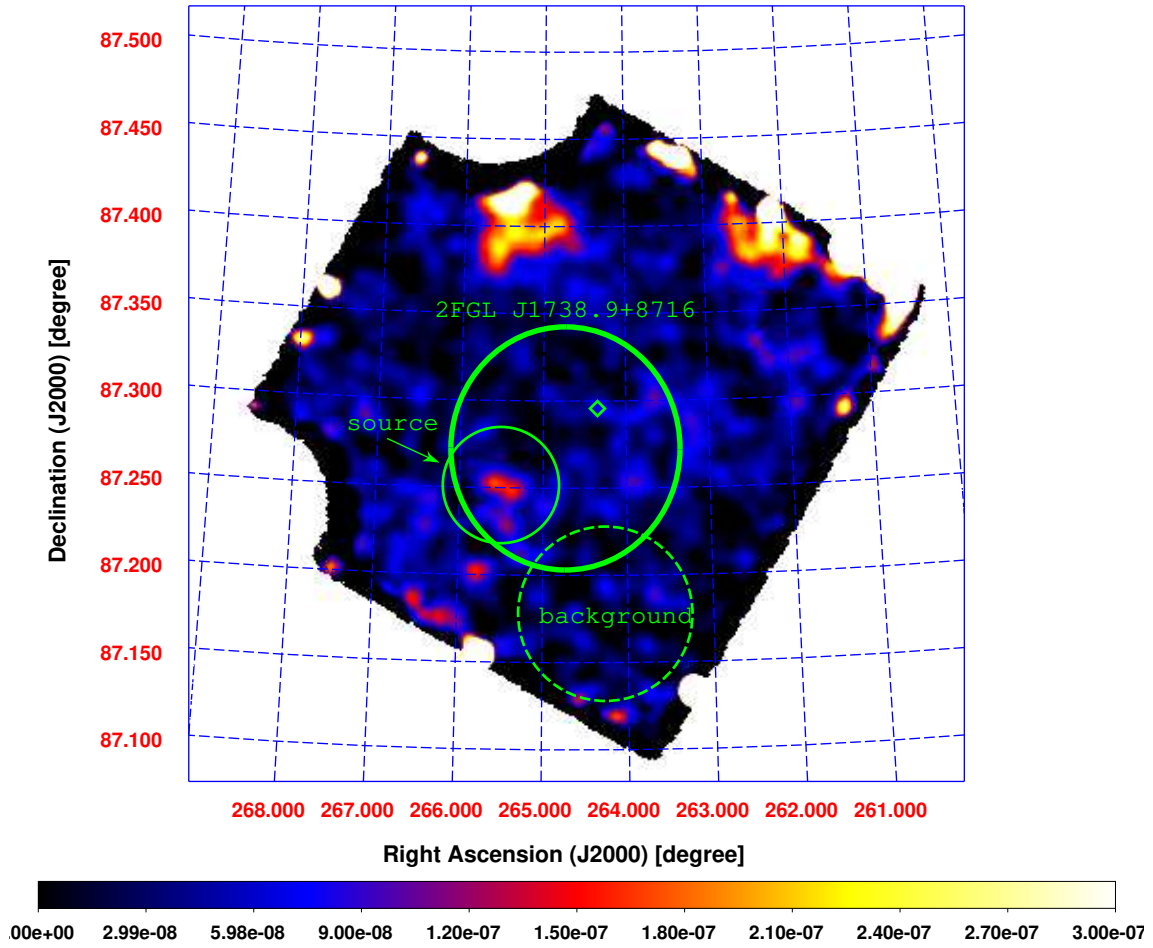


Fig. 4.— X-ray image of 1FGL J1739.4+8717 by *Suzaku*/XIS0+3 (FI CCDs) in the 0.5 to 10 keV energy band. Thick solid ellipse denotes the 95% position error of the 2FGL catalog counterpart of 1FGL J1739.4+8717. Thin solid and dashed circles show the source and background regions, respectively. The radio position of NVSS J173722+871744 is marked with a green rhombus.

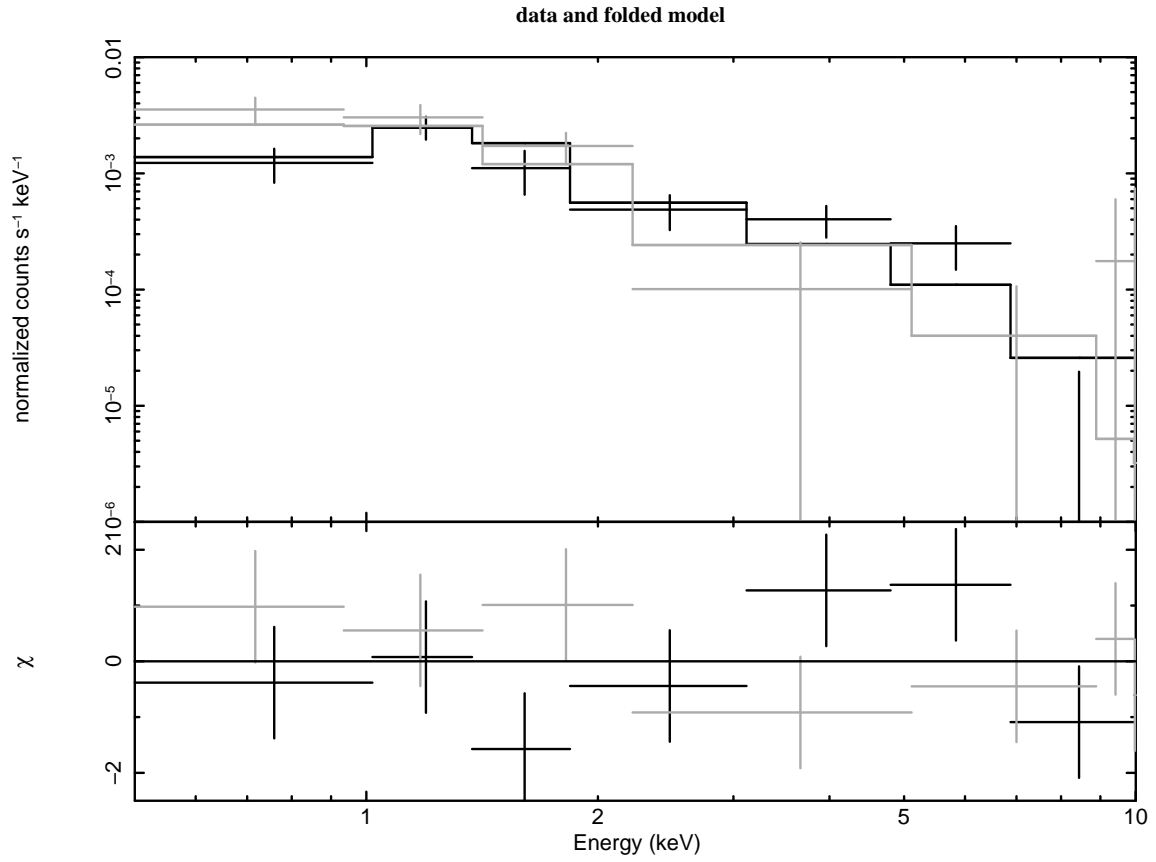


Fig. 5.— X-ray spectrum of the X-ray counterpart of 1FGL J1739.4+8717 fitted with a power-law model. Black plots show the FI data and gray plots show the BI data.

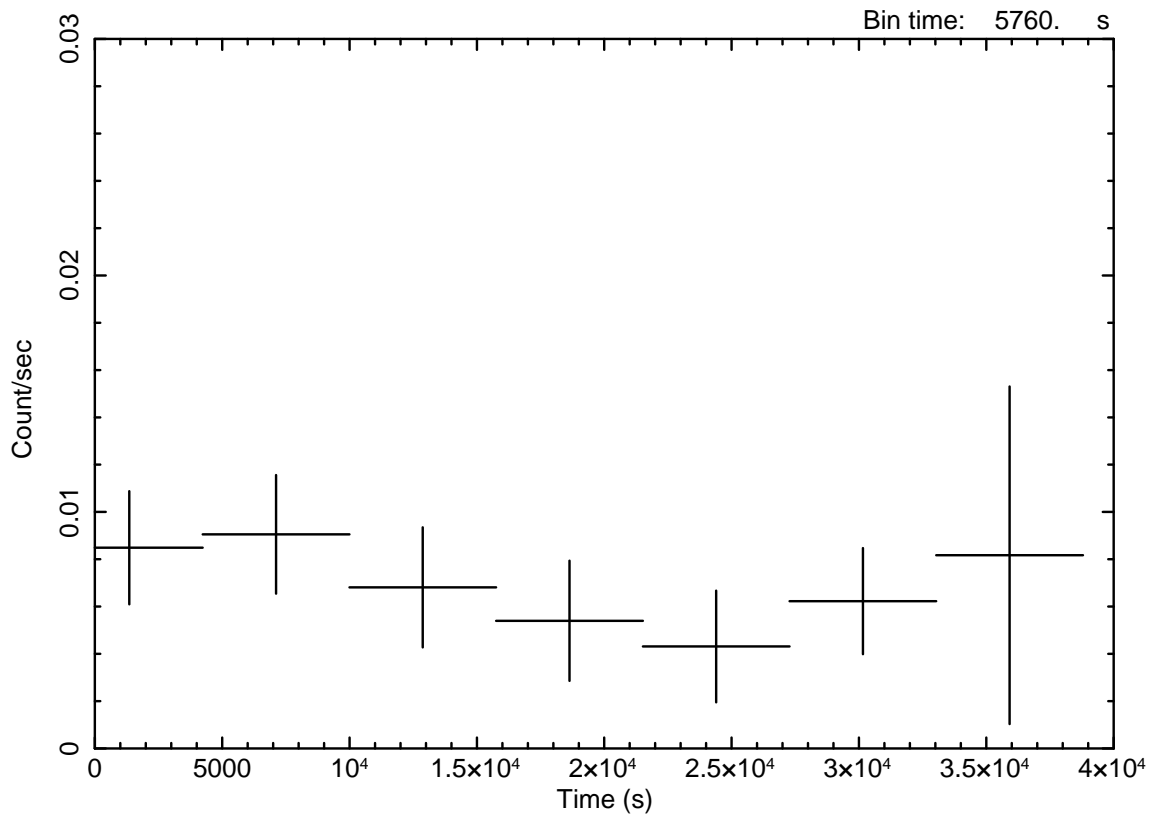


Fig. 6.— *Suzaku* /XIS light curve of the X-ray counterpart of 1FGL J1739.4+8717.

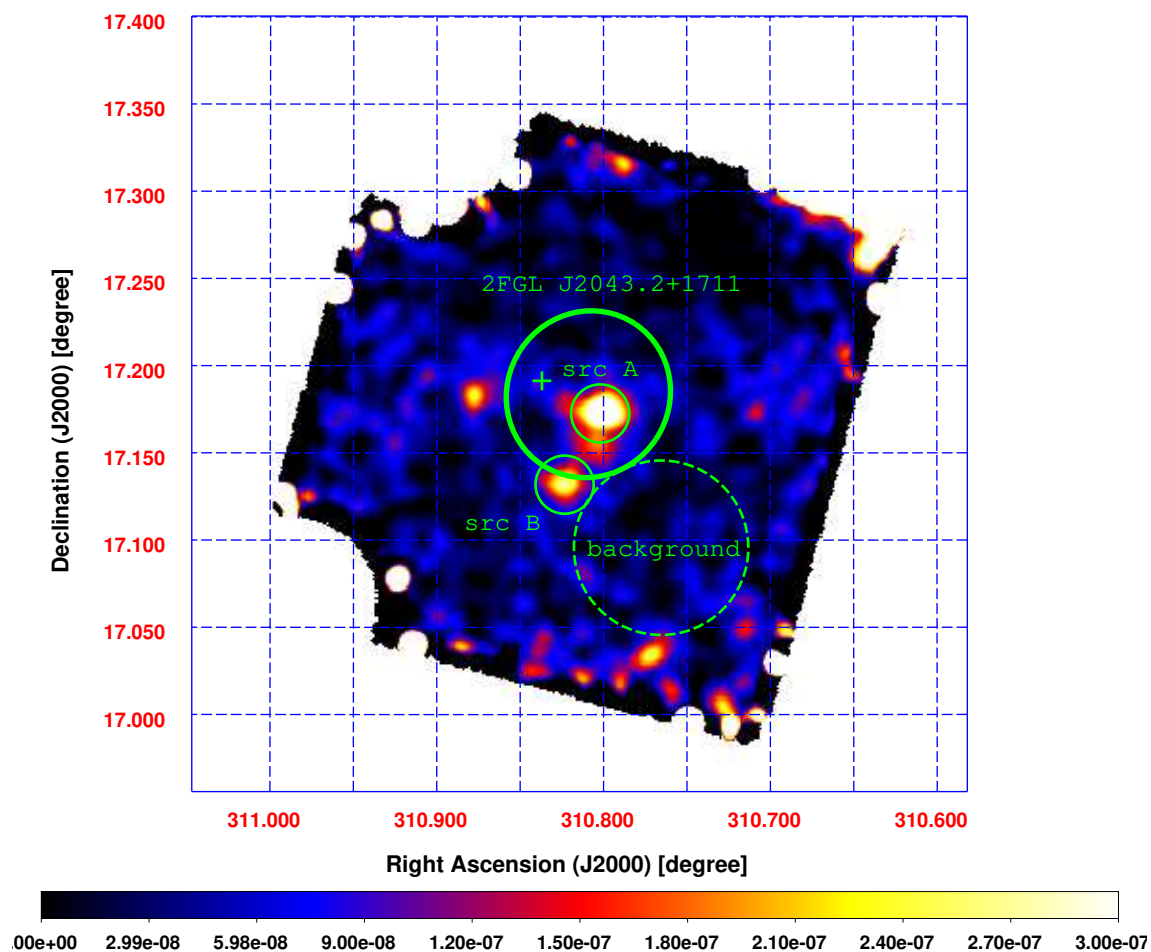
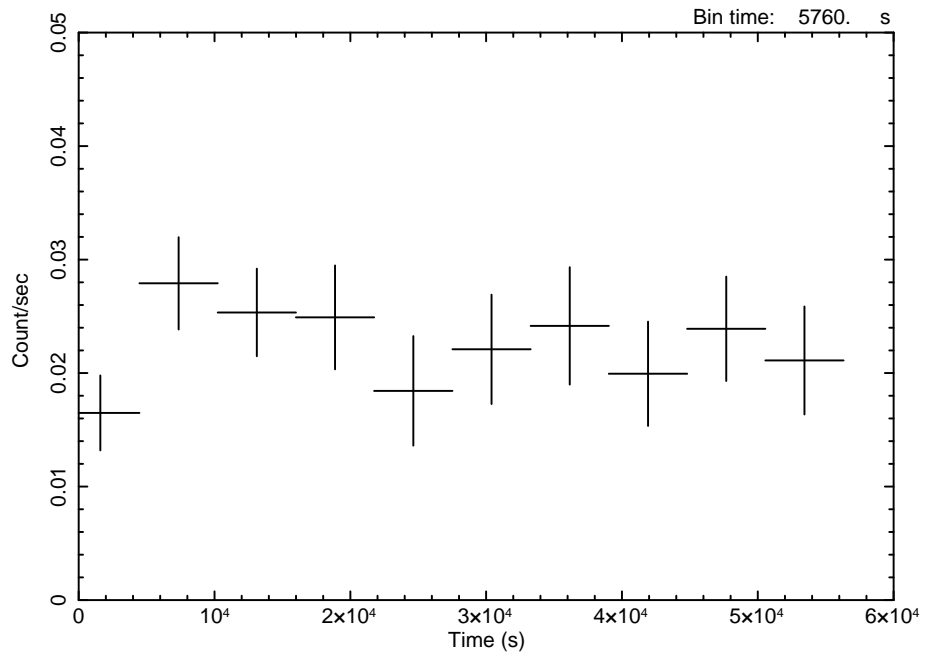
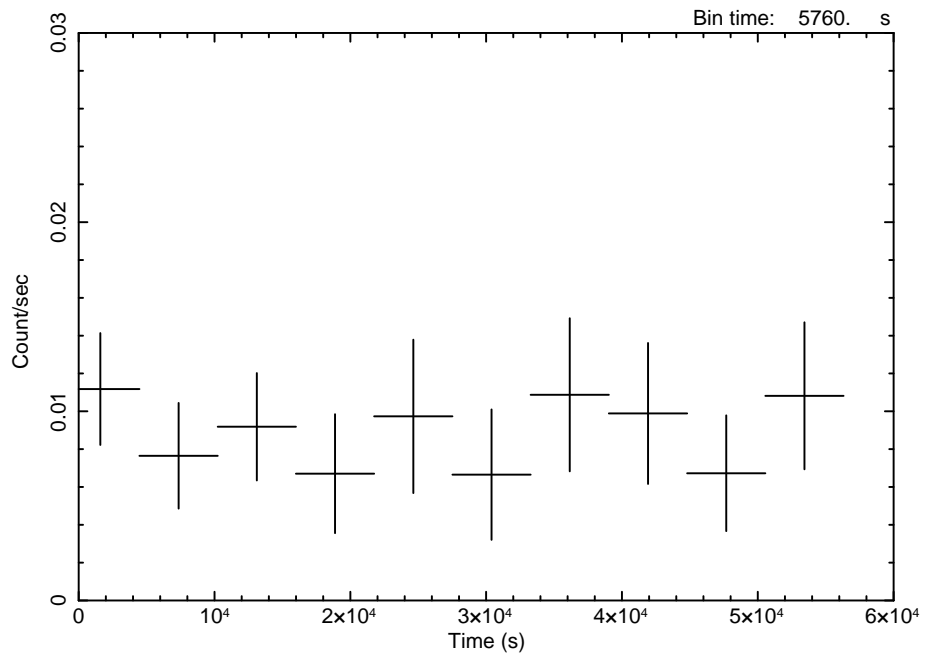


Fig. 7.— X-ray image of 1FGL J2043.2+1709 by *Suzaku*/XIS0+3 (FI CCDs) in the 0.5 to 10 keV energy band. The thick solid ellipse denotes the 95% position error of 1FGL J2043.2+1709 from the 2FGL catalog. Thin solid and dashed circles show the source and background regions, respectively. Two X-ray sources inside the positional error ellipse of 1FGL J2043.2+1709 are named srcA for the northern source and srcB for the southern source. The position of the associated MSP PSR J2043+1711 is marked with a cross.

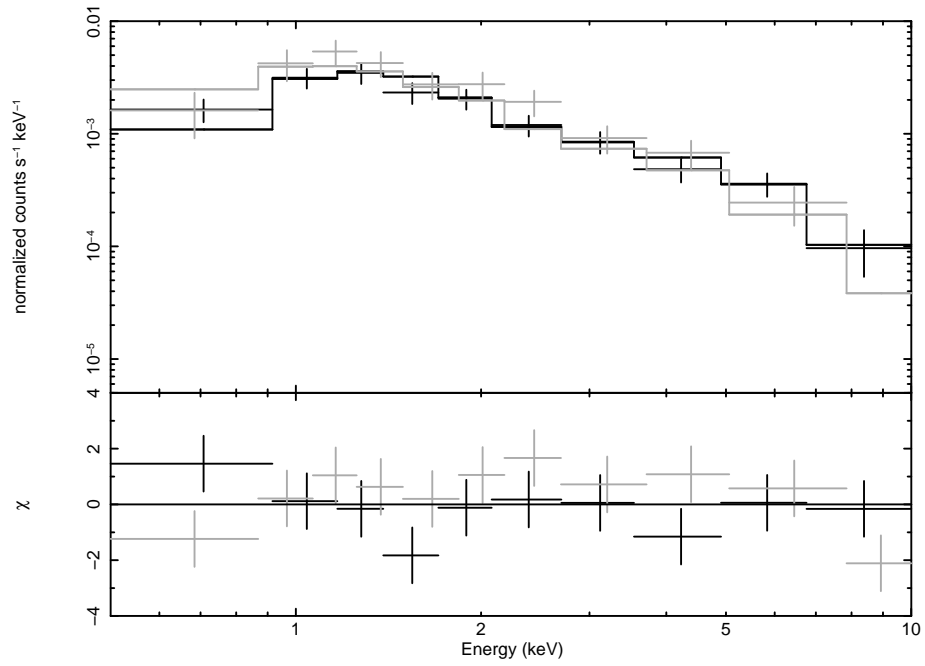


(a) Source A

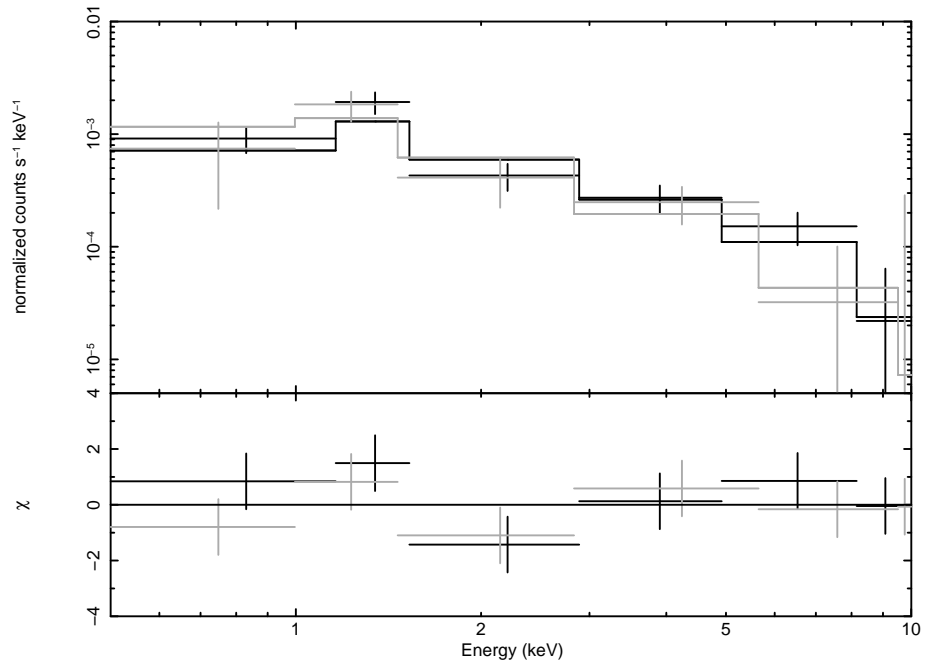


(b) Source B

Fig. 8.— *Suzaku*/XIS light curve of srcA (a) and srcB (b).



(a) Source A



(b) Source B

Fig. 9.— *Suzaku*/XIS spectra of srcA (a) and srcB (b) inside the error ellipse of 1FGL J2043.2+1709. Both spectra are fitted with an absorbed power-law model. Black plots show the FI data and gray plots show the BI data.

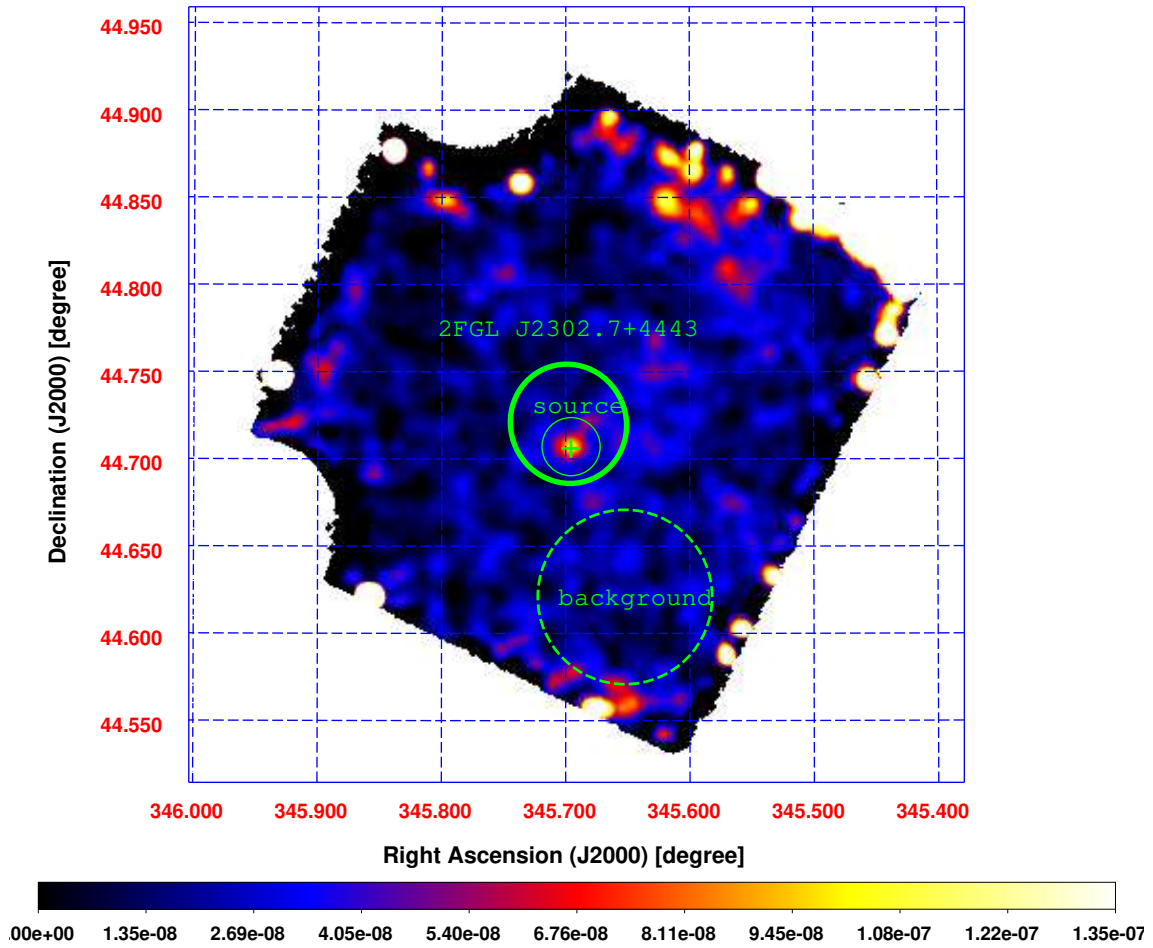


Fig. 10.— X-ray image of 1FGL J2302.8+4443 by *Suzaku*/XIS0+3 (FI CCDs) in the 0.5 to 2 keV energy band. Thick solid ellipse denotes 95% position error of 1FGL J2302.8+4443 from the 2FGL catalog. Thin solid and dashed circles show the source and background regions, respectively. The position of the associated MSP PSR J2302+4442 is marked with a cross.

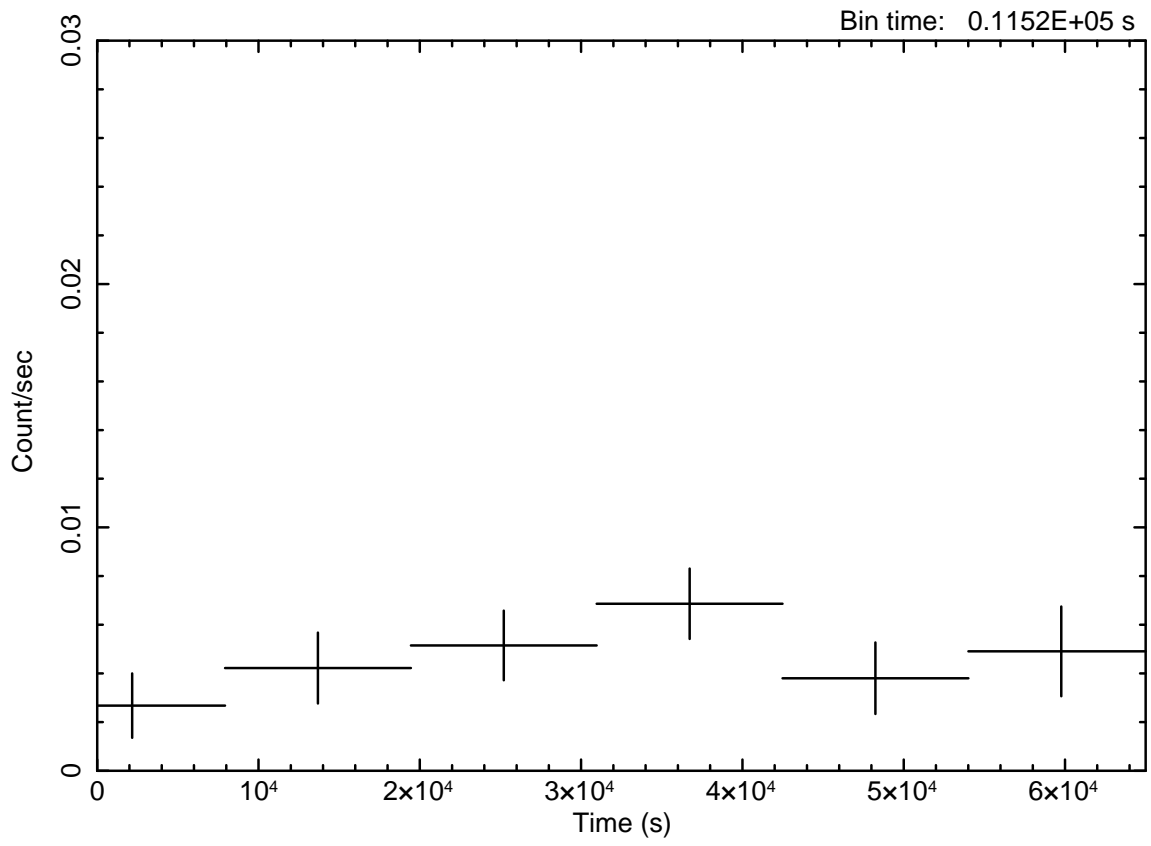


Fig. 11.— *Suzaku*/XIS light curve of the X-ray counterpart of 1FGL J2302.8+4443.

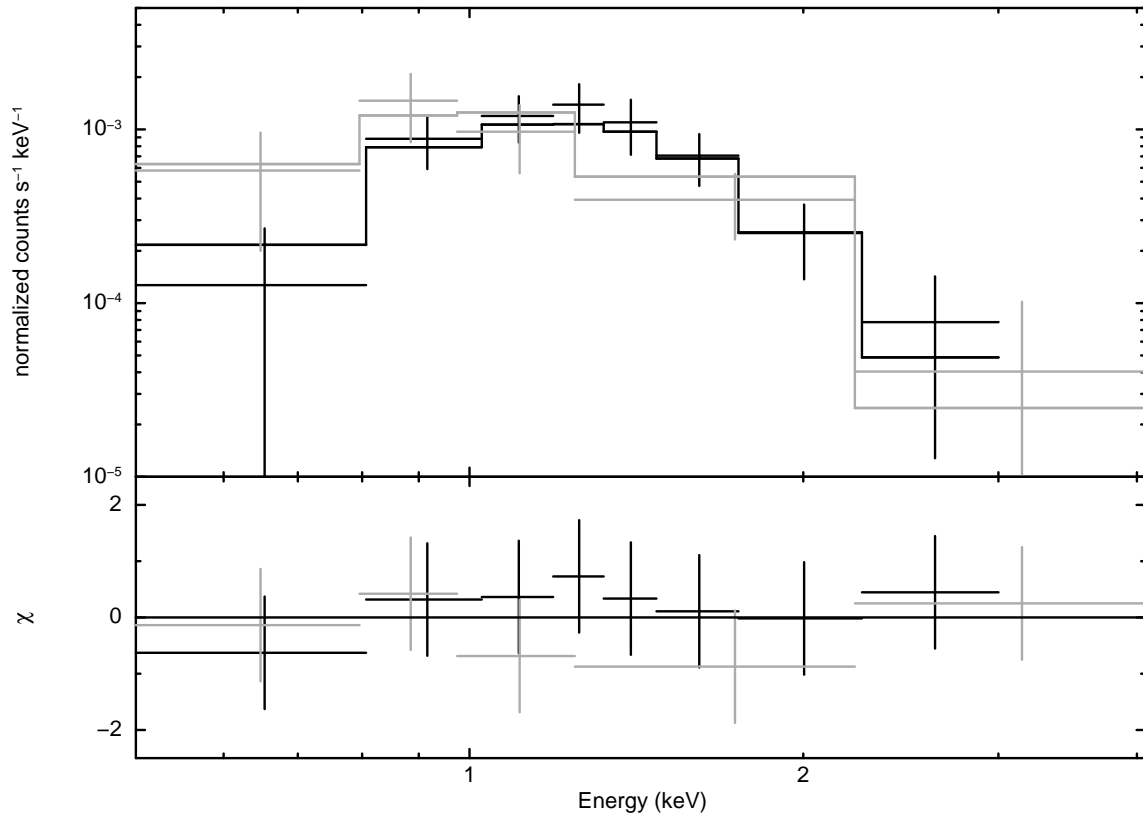


Fig. 12.— *Suzaku*/XIS spectrum of the X-ray counterpart of 1FGL J2302.8+4443 fitted with a black body model. Black plots show the FI data and gray plots show the BI data.

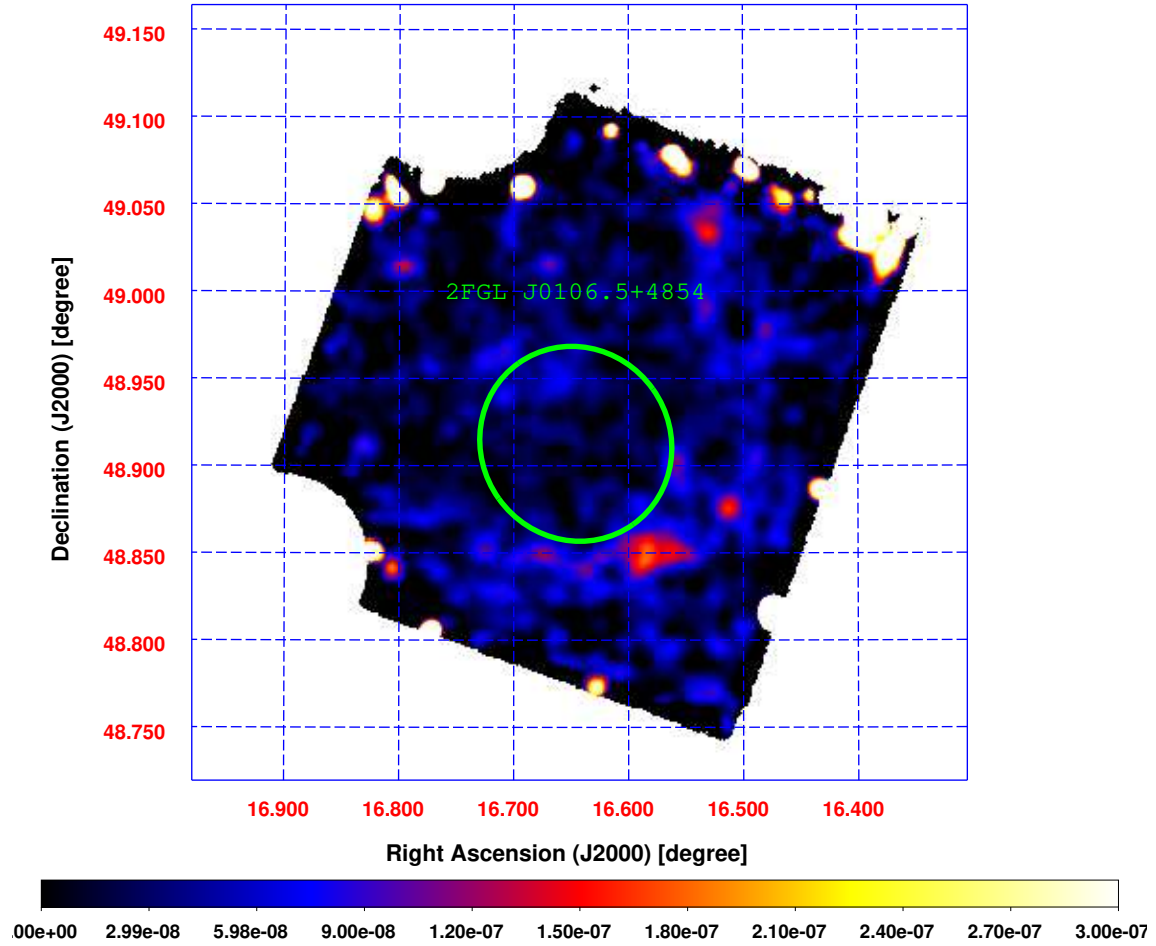


Fig. 13.— X-ray image of 1FGL J0106.7+4853 by *Suzaku*/XIS0+3 (FI CCDs) in the 0.5 to 10 keV energy band. Thick solid ellipse denotes 95% position error of 1FGL J0106.7+4853 from the 2FGL catalog.

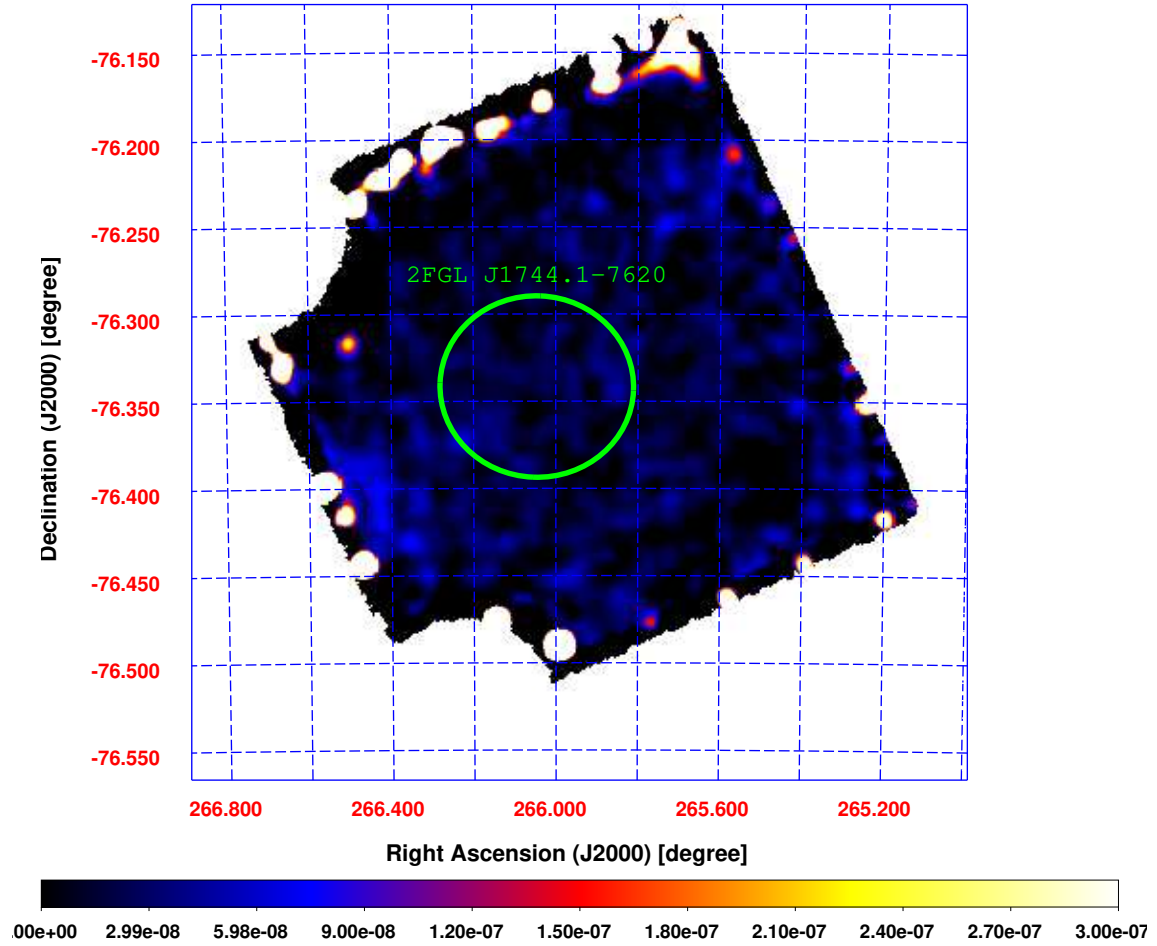


Fig. 14.— X-ray image of 1FGL J1743.8–7620 by *Suzaku*/XIS0+3 (FI CCDs) in the 0.5 to 10 keV energy band. Thick solid ellipse denotes 95% position error of 1FGL J1743.8–7620 from the 2FGL catalog.

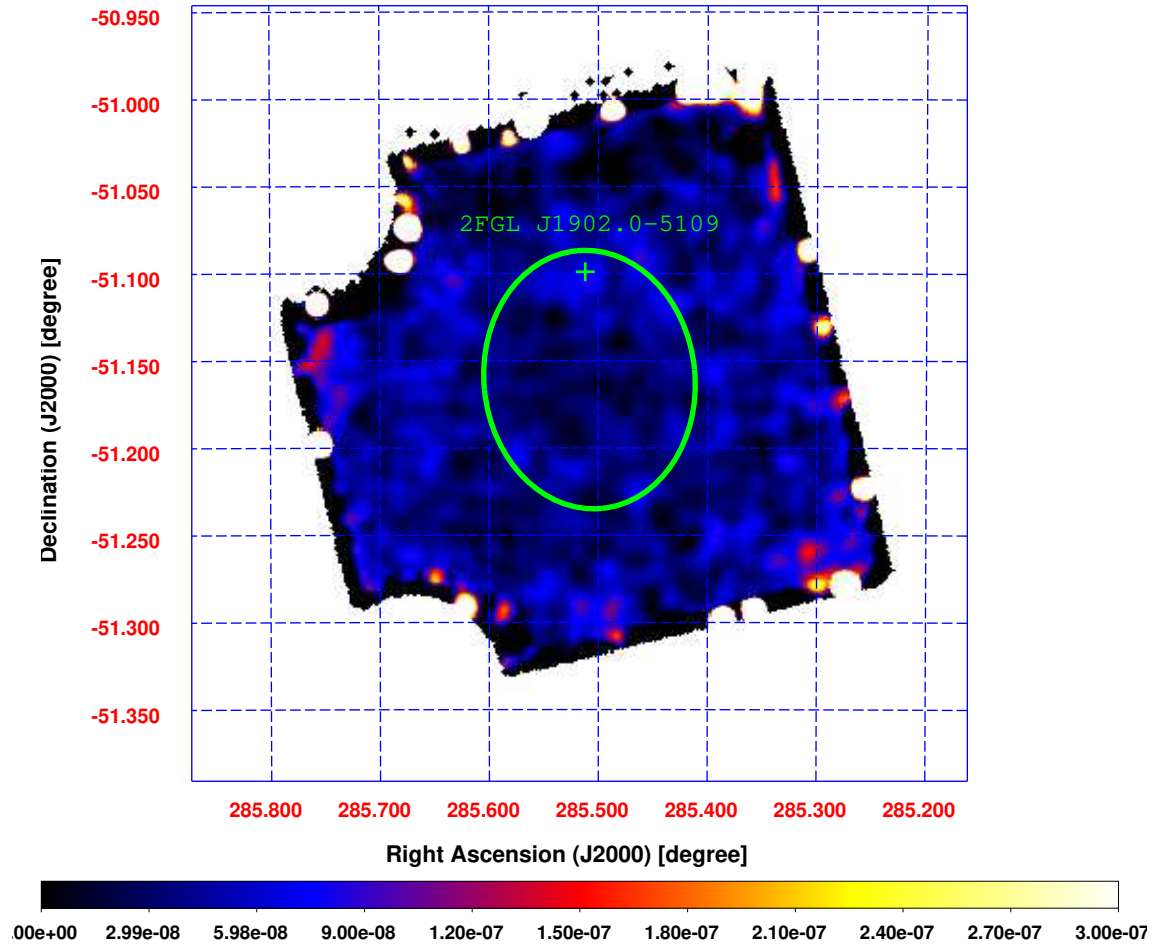


Fig. 15.— X-ray image of 1FGL J1902.0–5110 by *Suzaku*/XIS0+3 (FI CCDs) in the 0.5 to 10 keV energy band. Thick solid ellipse denotes 95% position error of 1FGL J1902.0–5110 from the 2FGL catalog. The accurate position of PSR J1902–5105 is still not available in the literature.

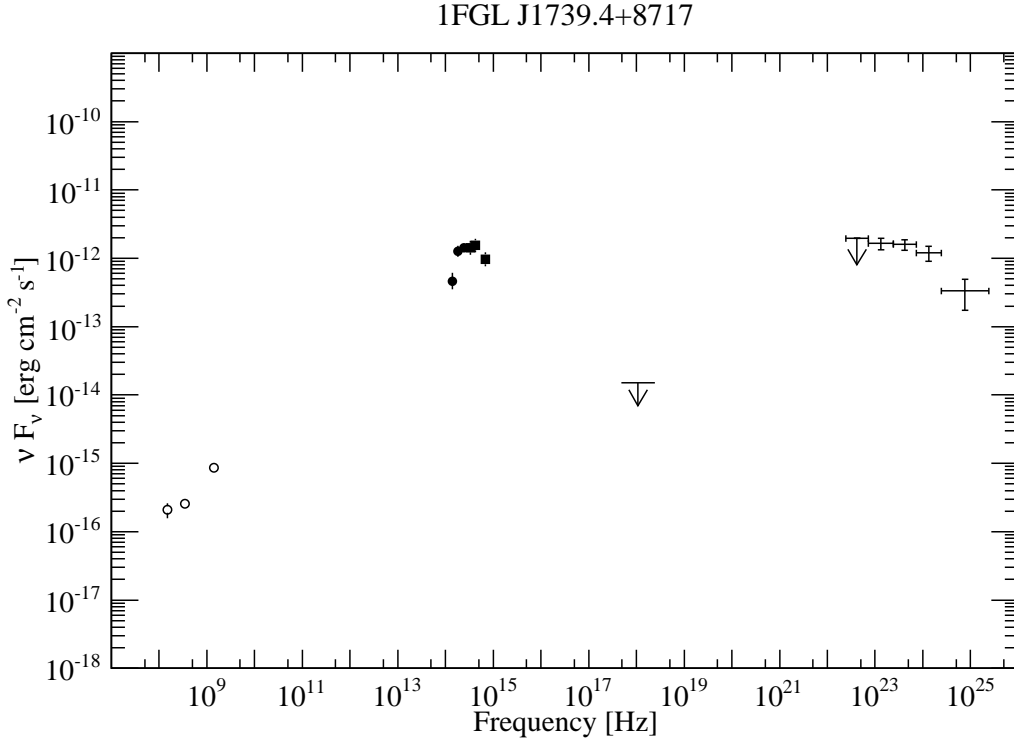


Fig. 16.— Spectral energy distributions of 1FGL J1739.4+8717. The X-ray data represents 90% confidence upper limit calculated from our *Suzaku* data. The γ -ray data points are taken from the 1FGL catalog (Abdo et al. 2010b). The radio data points are 6C B175708+871924 in 6C catalog (Baldwin et al. 1985), WENSS B1758.4+8718 in WENSS catalog (Rengelink et al. 1997) and NVSS J173722+871744 in NVSS catalog (Condon et al. 1998). Infrared and optical plots, 2MASS J17372480+8717433 and USNOB 1772-0020476, are quoted from 2MASS point source catalog (Skrutskie et al. 2006) and USNO B1.0 catalog (Monet et al. 2003), respectively.

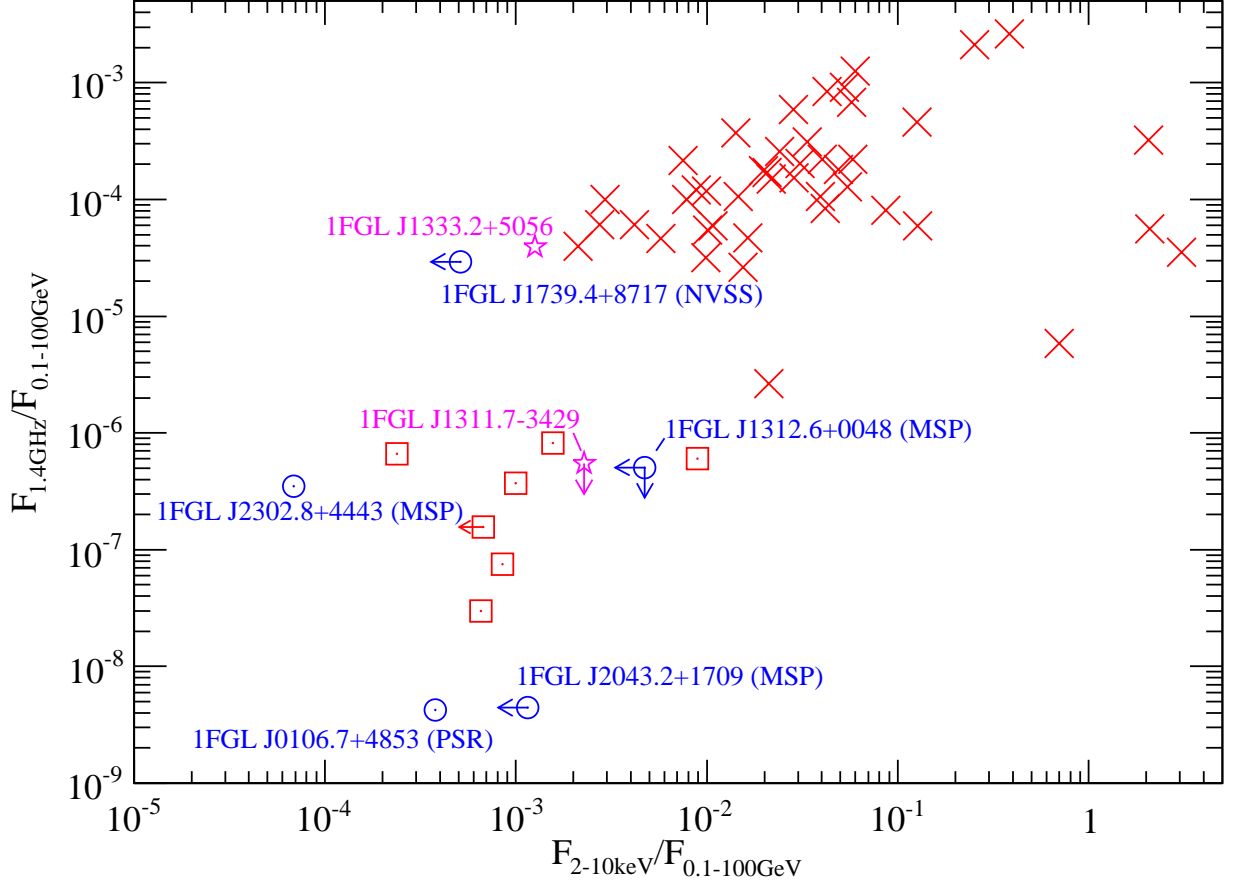


Fig. 17.— X-ray to γ -ray flux ratios versus radio to γ -ray flux ratios for unassociated *Fermi*-LAT sources. The blue circles show the flux ratios of unassociated *Fermi*-LAT sources which we observed using the *Suzaku* satellite. The γ -ray flux and the radio upper limits of these sources are taken from values of the 1FGL catalog and the NVSS catalog (Condon et al. 1998), respectively. Red x marks indicate the data plots of blazars listed in Abdo et al. (2010f). Red squares represent the data points of the *Fermi*-LAT sources that are associated with MSPs discovered by Cognard et al. (2011) and Ransom et al. (2011), and three *Fermi*-LAT sources listed in Abdo et al. (2010j) for which the best fit model of the X-ray spectra were determined. The values of X-ray flux and radio fluxes of MSPs in Abdo et al. (2010j) are quoted and derived from Bailes et al. (1997), Lundgen et al. (1995), Navarro et al. (1995), Sakurai et al. (2001), Webb et al. (2004a), and Webb et al. (2004b). For the MSPs we cannot quote the radio flux at 1.4 GHz, we estimated 1.4 GHz flux by the extrapolation using radio fluxes that are available in the literature assuming a power-law model. Pink stars show the two still unassociated 1FGL sources from our first year campaign targets (Maeda et al. 2011) and another two 1FGL sources studied in Maeda et al. (2011) and that are now associated with MSPs are involved in red squares.